Received: 14 June 2019 | Revised: 10 April 2020 | Accepted: 7 May 2020

DOI: 10.1002/ldr.3652

WILEY

RESEARCH ARTICLE

Monitoring Matang's Mangroves in Peninsular Malaysia through Earth observations: A globally relevant approach

Richard Lucas[1,2] | Viviana Otero[3] | Ruben Van De Kerchove[4] | David Lagomasino[5] | Behara Satyanarayana[3,6] | Temilola Fatoyinbo[7] | Farid Dahdouh-Guebas[3,8]

[1]Department of Geography and Earth Sciences, Aberystwyth University, Aberystwyth, UK

[2]School of Biological, Earth and Environmental Sciences (BEES), University of New South Wales (UNSW), Kensington, New South Wales, Australia

[3]Systems Ecology and Resource Management Research Unit, Department of Organism Biology, Université Libre de Bruxelles (ULB), Brussels, Belgium

[4]Remote Sensing, Vlaamse Instelling Voor Technologisch Onderzoek (VITO) Research Organisation, Mol, Belgium

[5]Department of Coastal Studies, East Carolina University, Greenville, North Carolina

[6]Mangrove Research Unit (MARU), Institute of Oceanography and Environment, Universiti Malaysia Terengganu (UMT), Kuala Nerus, Malaysia

[7]NASA Goddard Space Flight Center, Biospheric Sciences Laboratory, Greenbelt, Maryland

[8]Laboratory of Plant Biology and Nature Management, Ecology and Biodiversity, Vrije Universiteit Brussel (VUB), VUB-APNA-WE, Brussels, Belgium

Correspondence
Richard Lucas, Department of Geography and Earth Sciences, Aberystwyth University, Aberystwyth, Ceredigion SY23EJ, UK
Email: richard.lucas@aber.ac.uk

Funding information
Federaal Wetenschapsbeleid, Grant/Award Number: SR/00/323

Abstract

Expansion of rotational timber harvesting of mangroves is set to increase, particularly given greater recognition of the economic, societal and environmental benefits. Generic and standardized procedures for monitoring mangroves are, therefore, needed to ensure their long-term sustainable utilisation. Focusing on the Matang Mangrove Forest Reserve (MMFR), Perak State, Peninsular Malaysia, thematic and continuous environmental descriptors with defined codes or units, including lifeform, forest age (years), canopy cover (%), above-ground biomass (Mg ha^{-1}) and relative amounts of woody debris (%), were retrieved from time-series data from spaceborne optical and single/dual polarimetric and interferometric RADAR. These were then combined for multiple points in time to generate land cover and evidence-based change maps according to the Food and Agriculture Organisation (FAO) Land Cover Classification System (LCCS) and using the framework of the Earth Observation Data for Ecosystem Monitoring (EODESM). Change maps were based on a pre-defined taxonomy, with focus on clear cutting and regrowth. Uncertainties surrounding the land cover and change maps were based on those determined for the environmental descriptors used for their generation and through comparison with independent retrieval from other EO data sources. For the MMFR and also for other mangroves worldwide where harvesting is occurring or being considered, a new approach and opportunity for supporting management of mangroves is presented, which has application for future planning of mangrove resources.

KEYWORDS

classification, management, mangroves, monitoring, remote sensing

1 | INTRODUCTION

Mangrove forests occupy the coastal regions of over 120 countries (Spalding, Kainuma, & Collins, 2010) and these forests represent a major resource for local and national populations. This was emphasised in the United Nations Ocean Conference in 2017, which highlighted that nearly one billion people are living in coastal communities, many of these are in the tropics and subtropics and in areas supporting mangroves. In these regions, there is considerable interest in increasing the extent and cover of mangrove forests across their potential range whilst ensuring economic returns for local communities and maximising national and international economic, societal, political and

environmental benefits (Bosire et al., 2008; Rönnbäck, Crona, & Ingwall, 2007). Maintaining and restoring mangroves are sensible options that have been increasingly recognised by national governments and the international community, with emphasis placed on ensuring exploitation is sustainable and addresses the well-being of current and future generations (Bosire et al., 2008; Ellison, 2000; Goessens et al., 2014; Huge et al., 2016; Satyanarayana et al., 2017). These options are particularly relevant given the rapid and unprecedented changes in global climate and the need to retain and expand carbon stocks and sinks, address resource demands in coastal regions and particularly where human populations are increasing, and guarantee protection of ecosystem values and services, including those related to biodiversity (Alongi, 2008; Alongi, 2012; Spalding et al., 2010; Walters et al., 2008).

Options for generating a sustainable and viable revenue stream from mangroves include rotational timber production, ecotourism (e.g., through conservation) and planned use of resources embedded within or linked to this ecosystem (e.g., invertebrate and fish populations, carbon stocks) (Alongi, 2012; Ellison, 2000; López-Portillo et al., 2017; Walton, Samonte-Tan, Primavera, Edwards-Jones, & Le Vay, 2006). Recognising the financial impacts of not maintaining a mangrove cover is also important as these can be substantive and include costs associated with restoring infrastructure and other resources lost following, for example, storms, flooding and sea-level rise (Costanza et al., 1997; Di Nitto et al., 2014; Lee et al., 2014). For this reason, there is a need to better understand the characteristics of their landscape settings, quantify current and past extents, dynamics and values of mangrove forests (with reference to biophysical attributes), be better informed regarding pathways for development and have capacity to predict future resource availability and benefits (Lee et al., 2014; Thomas et al., 2017).

Such efforts have been significantly advanced with the release of up-to-date maps of regional and global mangrove extent (Bunting et al., 2018), height (Fatoyinbo & Simard, 2013), biomass (Simard et al., 2019) and restoration potential (Worthington & Spalding, 2018) as well as mudflat extent (Murray et al., 2019). These baselines provide new opportunities for ongoing monitoring of mangroves and their environs. However, there is a need also to concurrently establish routine, standardized and consistent methods for (a) understanding historical, current and future dynamics of mangroves in response to different drivers of change, whether these be natural (e.g., Duke et al., 2017) or anthropogenic (e.g., Richards & Friess, 2016; Thomas et al., 2017) and (b) informing communities, landholders and governments of mangrove values and progress toward their sustainable management, restoration, conservation and use (e.g., Huge et al., 2016; Kairo, Dahdouh-Guebas, Bosire, & Koedam, 2001; Satyanarayana et al., 2012). Considering the additional danger posed by cryptic ecological degradation (Dahdouh-Guebas et al., 2005), Koedam and Dahdouh-Guebas (2008) highlighted the urgent need for creating an early warning system for detecting ecological quality changes and degradation in mangrove forests.

Focusing on the Matang Mangrove Forest Reserve (MMFR) in Perak State, Peninsular Malaysia, this research aimed to establish and demonstrate a globally applicable, viable and robust framework for monitoring commercially managed mangroves using satellite sensor data. As components, the framework needed to facilitate historical overviews and understanding of the impacts of past and ongoing management, identify changes that were both historical in nature but also as and when new satellite data become available, and inform on potential future changes. To achieve this aim, the methods associated with the Earth Observation Data for Ecosystem Monitoring (EODESM; Lucas & Mitchell, 2017) were used, with this being an advance on its predecessor, the Earth Observation Data for Habitat Monitoring (EODHaM: Lucas et al., 2014). EODESM generates maps of land cover and changes according to the Food and Agriculture Organisation (FAO) Land Cover Classification System (LCCS; Version2), and by integrating environmental descriptors (EDs) retrieved primarily from Earth observation (EO) data.

The MMFR was selected because the *Rhizophora*-dominated forests have been managed for charcoal and pole production since 1902, making the reserve one of the longest silvicultural management areas globally (Chong, 2006; Muda & Nik Mustafa, 2003). The changes in mangrove cover in the MMFR are rapid because of the nominal 30-year forest rotation cycle and the MMFR was, therefore, well suited for monitoring using EO (e.g., Aziz, Phinn, Dargusch, Omar, & Arjasakusuma, 2015; Otero et al., 2019). The clearances and the progression of the logging cycle have also been shown to be readily identifiable within 30 m resolution Landsat and approximately 18 m resolution Japanese L-band Synthetic Aperture RADAR (SAR) data and these have proved useful for mapping mangrove extent in the MMFR and for retrieving EDs (Lucas et al., 2020). Otero et al. (2019) also determined the advantages of using Landsat sensor data and derived indices for ageing forests and understanding dynamics associated with the management process. Otero et al. (2018) and Lucas et al. (2020) further identified the role that unmanned airborne vehicles (UAVs) can play in providing more detailed and supportive information on several EDs (e.g., canopy height). Whilst this study served primarily to support ongoing management of forests in the MMFR by the Malaysian Forestry Department, the approach was developed such that it was relevant and applicable to other areas where future harvesting is taking place or is proposed (e.g., in Malaysia and Indonesia, including West Papua and the Arafura Sea mangrove area; Chong, 2006, Sillanpaa, Vantellingen, & Friess, 2017).

2 | STUDY AREA

The MMFR (Figure 1) is located on the western coast of Peninsular Malaysia within the tropical monsoonal region (Köppen climate classification category of Am; mean monthly temperatures exceeding 18° in every month and a dry season) and occupies an area of approximately 40,000 ha (Ariffin & Mustafa, 2013). The area receives an annual rainfall ranging from 2,000 to 2,800 mm and average air temperatures ranges from 22 to 33°C (Ariffin & Mustafa, 2013). Being protected from ocean waves and tidal influences (spring tide amplitude of 3.3 m) (Ashton, Hogarth, & Ormond, 1999), the MMFR has extensive mangrove forests that colonise and thrive along the coastline of ~51.5 km (Goessens et al., 2014).

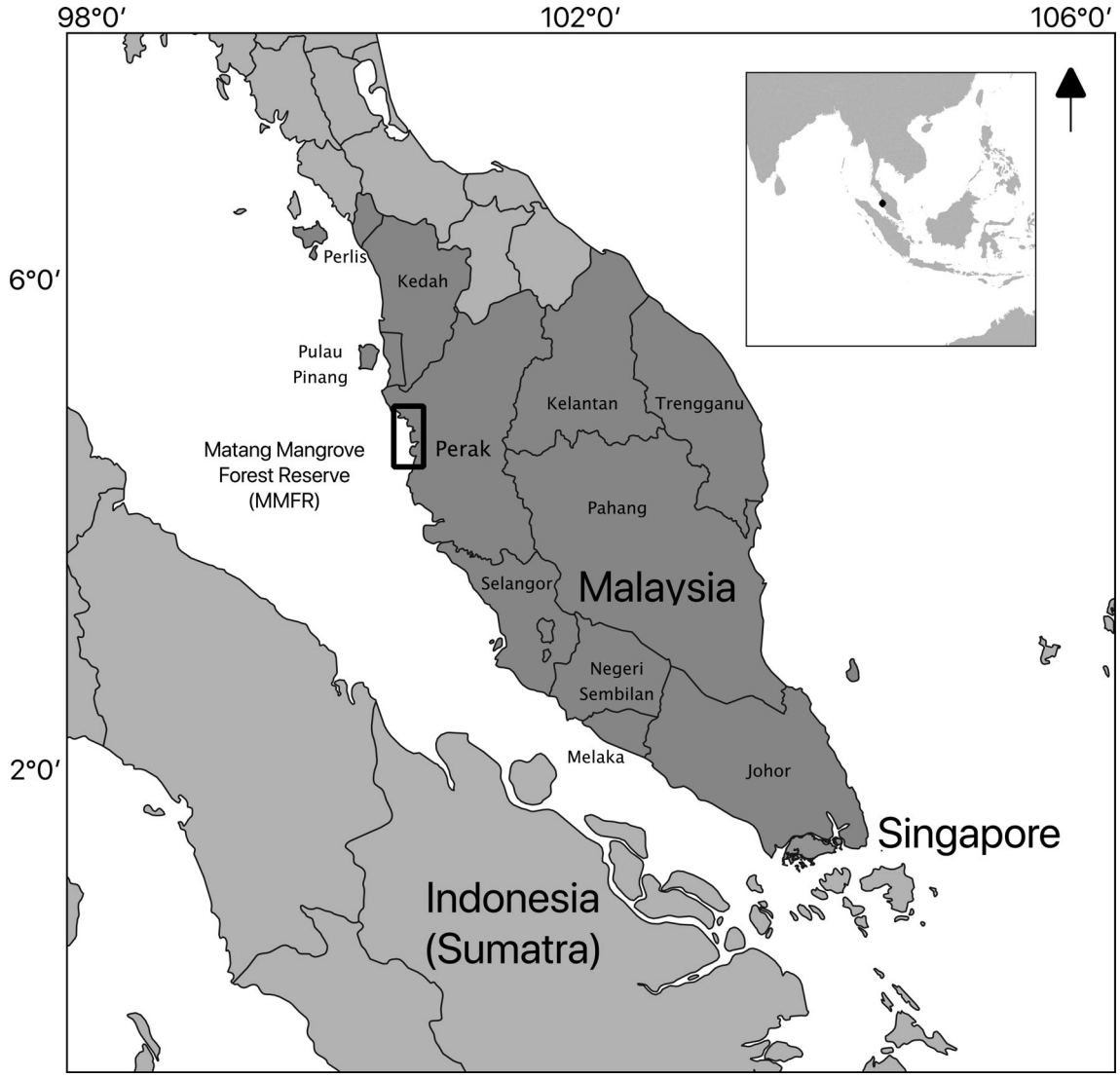

FIGURE 1 The location of the Matang Mangrove Forest Reserve (MMFR) in Peninsular Malaysia. Map adapted from Weidmann, Kuse, and Gleditsch (2010)

The management divides the area of the MMFR into four zones: protective, productive, restrictive productive and unproductive (Ariffin & Mustafa, 2013). The productive and restrictive productive zones are managed under a 30-year rotation cycle and are the areas where timber extraction takes place. These zones are mainly composed of *Rhizophora apiculata* Blume and *R. mucronata* Lamk. (Ariffin & Mustafa, 2013). Within the productive and restrictive productive forests, the logging cycle involves clear-felling of the coupes. Areas between 2.2 and 6.6 ha are assigned by the local management to different charcoal contractors that perform the clear-felling operations (Ariffin & Mustafa, 2013) over the course of approximately 24 months (Lucas et al., 2020). The timber is removed but the remnants of the cut stumps, primarily the prop roots of the dominant *R. apiculata* and *R. mucronata*, and woody debris (branches and some trunks) remain. After cutting, subsequent forest growth in coupes takes place through natural regeneration assisted by planting if needed, with the extent and production assessed after 2 years of growth. After approximately 15 and 20 years of growth, the forests are typically thinned (Ariffin & Mustafa, 2013) and eventually recleared once the forests have reached maximum productivity (i.e., at approximately 30 years). The Forestry Department has favoured the establishment of the two *Rhizophora* species previously mentioned, with these being pest-resistant and highly calorific. This has resulted in relatively even-aged monocultures. However, within the MMFR, 25 other mangrove species occur although these are largely confined to the protective zones (Ariffin & Mustafa, 2013).

3 | METHODS

3.1 | Available data

For the present study, all available LANDSAT Thematic Mapper (TM) and Enhanced TM (ETM+) surface reflectance data (%) over the period 1988–2016 were obtained from the United States Geological

Survey (USGS; LANDSAT World Reference System Path 128, Row 57). The nominal spatial resolution is 30 m. Cloud-free LANDSAT scenes for individual dates were available for most years, with the exception of 2012 because of failure in the LANDSAT-7 ETM+ Scan Line Corrector. However, where cloud cover occurred in all images acquired in a particular year, composites were necessarily generated. This was achieved by first selecting the image in each year with the least amount of cloud and cloud shadow and then replacing affected pixels with those that were cloud-free in other images from the same year (Otero et al., 2019). On average, only 3% of pixels needed to be replaced within the images with the least cloud cover. The use of composites was considered acceptable given that clear felling of coupes takes place over several years and because of the evergreen nature of mangroves in the MMFR. It should be noted, however, that a seasonal response has been observed in mangroves in other regions (Pastor-Guzman, Dash, & Atkinson, 2018).

All available Japanese Earth Resources Satellite (JERS-1) SAR, Advanced Land Observing Satellite (ALOS) Phased Arrayed L-band SAR (PALSAR) and ALOS-2 PALSAR-2 data (nominally 18 m spatial resolution) were obtained through the Japanese Space Exploration Agency (JAXA) Kyoto and Carbon (K&C) Initiative. The JERS-1 SAR provided L-band horizontally (H) polarised transmitted and received (L_{HH}) data whilst the ALOS PALSAR series acquired data at both HH and vertically (V) received (HV) polarisations (L_{HV}). JERS-1 SAR data were obtained for the periods March 12, 1993, to August 26, 1997 (L_{HH} only; 20 scenes), ALOS PALSAR Fine Beam Single (FBS; L_{HH}) and Fine Beam Dual (FBD; L_{HH} and L_{HV}) for June 1, 2006, to January 23, 2011 (45 scenes), and ALOS-2 PALSAR-2 FBS and FBD for October 2, 2014, to September 29, 2016 (8 scenes). These corresponded to the periods when the sensors were in operation. Observations were not available from 1997 to early 2006 (a period of approximately 9 years) and late 2011–2014 (approximately 3.5 years). Scenes with both full and partial coverage of the MMFR were used. Three scenes were excluded as they encompassed only a very small part of the MMFR. All SAR data were calibrated to the backscattering coefficient (σ^o, dB – Shimada, Isoguchi, Tadono, & Isono, 2009; Lucas et al., 2020). The final dataset (98 scenes; Figure 2), therefore, consisted of annual Landsat sensor (July 29, 1988–March 18, 2016; 28 single or composite scenes) and all available Japanese L-band SAR data (70). NASA Shuttle RADAR Topographic Mission (SRTM) data (30 m spatial resolution) were acquired between February 11 and 22, 2000. Tandem-X data (2011–2015; 12.5 m spatial resolution) were also obtained for the MMFR and the surrounding landscapes. All datasets were finally resampled, using GDAL, to 12.5 m spatial resolution following pre-processing and calibration so as to align with that of the TanDEM-X (Lucas et al., 2020).

In July 2016, and as described by Otero et al. (2018) and Lucas et al. (2020), DJI Phantom 3 true colour (RGB) Unmanned Airborne Vehicle (UAV) imagery were obtained over nine 1 ha plots in the MMFR, from which <1 m spatial resolution orthomosaics and canopy height models (CHMs) were generated.

3.2 | Land cover classifications

Based on the concepts of EODESM, land cover classes according to the FAO LCCS taxonomy (Figure 3) were generated for all 98 observation dates from EDs retrieved from combinations of LANDSAT sensor, L-band SAR and interferometric SAR, with these relating primarily to vegetation. All processing were undertaken using PYTHON scripts and the RSGISLib software of Bunting, Clewley, Lucas, and Gillingham (2013). This included pixel-level segmentation of the MMFR area to a spatial resolution of 12.5 m, attribution of segments with ED data using Raster Attribute Tables (RAT) stored through the KEA image format (Clewley et al., 2014; Gillingham & Bunting, 2014), and the combining of EDs to form land cover classes defined by the FAO LCCS taxonomy. All EDs used for the classifications were retrieved using relationships established with the resampled data. A flow chart outlining the overall approach is given in Figure 4 and further details in EODESM can be found in Lucas and Mitchell (2017), Lucas et al. (2019) and other forthcoming publications.

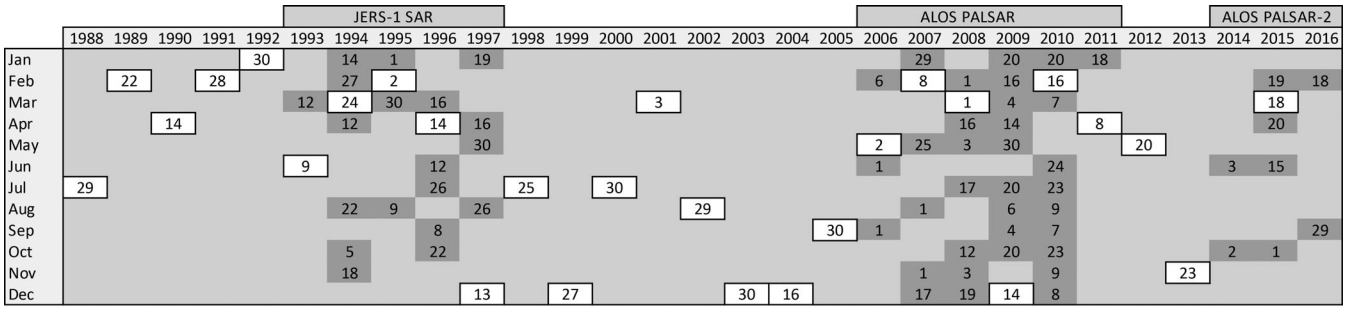

FIGURE 2 The 98 acquisition dates of JERS-1 SAR (1993–1997), ALOS PALSAR (2006–2011) and ALOS-2 PALSAR-2 (2015–2016) (grey) and LANDSAT sensor data (white) acquired for the MMFR. The numbers represent the dates of image acquisition. LANDSAT sensor and ALOS PALSAR data were acquired on March 1, 2018. ALOS PALSAR data were also acquired on the Apr 29, 2009, Aug 30 and Nov 30, 2007, March 14 and 18, 2009, Dec 5, 14 and 22, 2019, Dec 25, 2010 and Jan 23, 2011. The dates of acquisition SRTM, TanDEM-X and WORLDVIEW-2 data were February 11 and 22, 2000, mid-2015 (actual date unknown) and January 23, 2016, respectively

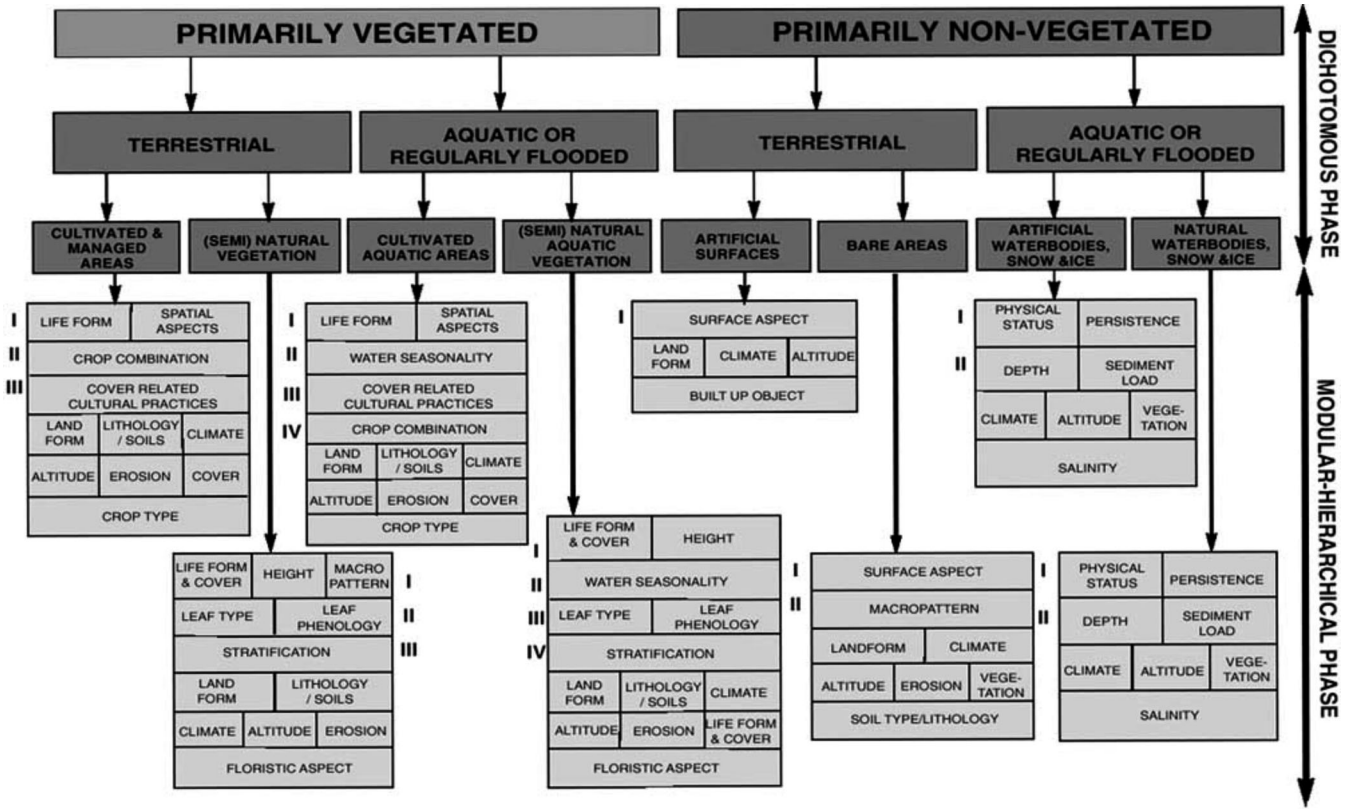

FIGURE 3 The LCCS Taxonomy (Taken from Di Gregorio & Jansen, 2000; Di, 2016)

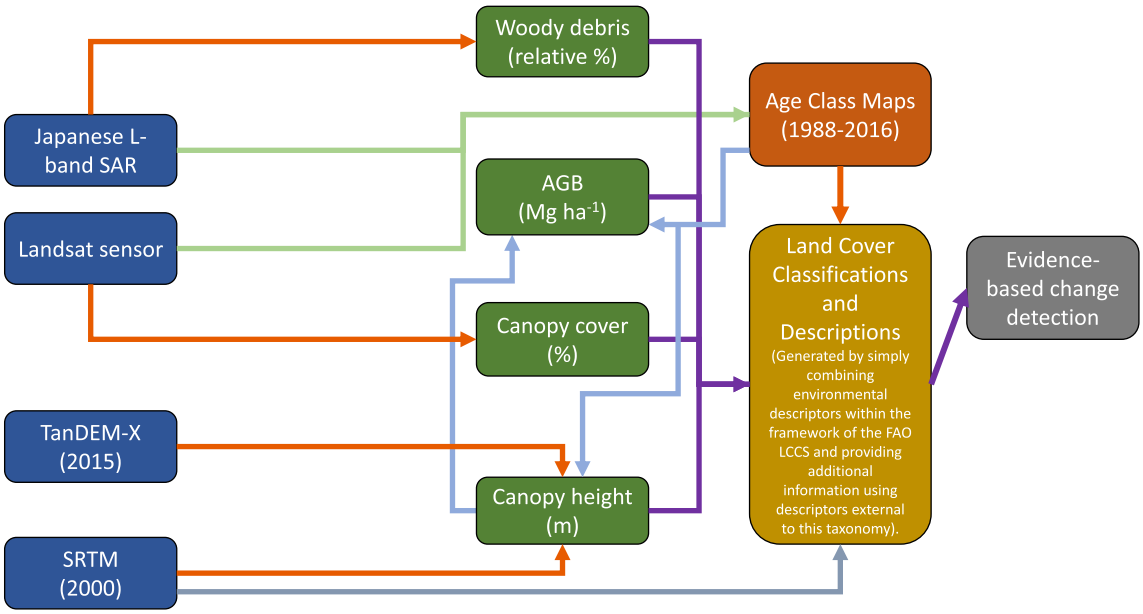

FIGURE 4 Flow chart outlining the steps taken to generate land cover and evidence-based change maps for the MMFR, with this involving generation of age class maps through time-series comparison of Japanese L-band SAR and LANDSAT sensor data (green arrows), retrieval of EDs from these satellite data (i.e., canopy cover and relative amounts of woody debris) and also interferometric SAR (canopy height; orange arrows), the use of relationships between canopy height, AGB and age (blue arrows) to estimate these EDs for each observation date, integration of all EDs to generate land cover classifications and descriptions and evidence-based change maps (purple arrows). The SRTM CHM was used to validate the age and canopy height estimates for 2000 (grey arrow) [Colour figure can be viewed at wileyonlinelibrary.com]

3.2.1 | Classification to FAO LCCS level 3

The generation of FAO LCCS Level 3 maps through EODESM required separate classification of five land cover types—primarily vegetated, aquatic, cultivated/managed, artificial surface and artificial water—with these assigned a value of 1. The inverse classes of primarily non-vegetated, terrestrial, semi-natural/natural, naturally bare surface or natural water were assigned a value of 0. The LCCS Level 3 classification was then generated through cross tabulation of these binary layers (Lucas & Mitchell, 2017).

For each of the 98 dates of observation, vegetated areas were identified as having a LANDSAT-derived Normalised Difference Moisture Index (NDMI) > 0.37 (range 0.32–0.39) or $L_{HH}\sigma^{o}$ < −8.0 dB (range −7.2 to −9.0 dB). These thresholds were determined for each date through visual interpretation of each LANDSAT or L-band SAR image and by referencing scenes acquired on the dates prior to and following. Variability in the thresholds was low and was attributed to prevailing conditions at the time of the satellite sensor observations, including tidal inundation and precipitation that influenced the moisture contents of the vegetation and ground surface. Together with open water, all remaining areas of the MMFR land area were assigned to a non-vegetated category, with the majority occurring because of logging activities. These areas exhibited a lower NDMI, because of the lack of a vegetation (canopy) cover following clearing. The high $L_{HH}\sigma^{o}$ observed in these areas was attributed to enhanced scattering of microwaves from cut stumps and woody debris remaining on the ground surface (Lucas et al., 2020). The aquatic class (summarised for each year) encompassed areas of mangrove within the MMFR and all water bodies. Artificial surfaces, which consisted primarily of the town of Kuala Sepetang but encompassed other small settlements, were associated with pixels in the 2016 Landsat image with an NDMI <0 (Otero et al., 2019). This threshold was determined through reference to Open Street Map (OMS) data for the region. The urban extent was assumed to be constant for each preceding date in the time-series, which was justified as changes in area had minimal impact on the extent of mangrove forest. All cultivated areas were outside of the MMFR and so this class was excluded from the classification, and all water areas were considered to be natural. Following generation of the five layers representing the extent of vegetated, aquatic and cultivated/managed lands, artificial surfaces or artificial water and their opposites, LCCS classifications to Level 3 were produced from their combination for each of the 98 observation dates over the period 1987–2016.

3.3 | Classification based on LCCS level 4

Within each LCCS Level 3 class, further descriptions were provided by considering what is termed here the Level 4 taxonomy, with particular focus on the primarily vegetated natural/semi-natural and non-vegetated aquatic categories (see Figure 3). In this case, more specific EDs were used to create raster layers whose values corresponded to pre-defined string codes in the LCCS taxonomy (e.g., A4 for trees, B5 for >14 m, or A1 for water in the lifeform, canopy height and water state modules, respectively). These were then combined to generate codes and descriptive labels for the different land cover categories. Within this modular phase, mangroves were described on the basis of their canopy cover and height (from which physiognomic lifeform was described), leaf type and phenology. As an example, and of relevance to mangroves, the class A24.A3.A21.B5.C1.D1.E1, which is formed from the combinations of codes and written out in the RAT, describes 'aquatic (A24) trees (A3) that have an open to closed (40–100%) canopy (A21), are tall (>14 m; B5), continuous (C1), broadleaved (D1) and phenologically evergreen (E1).' Additional attributes would be 'on flooded land (tidal), dominated by *Rhizophora apiculata* with an AGB (Mg ha^{-1}) of 123 Mg ha^{-1}.' Non-vegetated classes included water (described on the basis of liquid state) and bare areas (unconsolidated material; primarily mud). A summary of the target EDs and their generation from EO data is provided in the following sections.

3.3.1 | Canopy cover (%)

Tree canopy cover represents the proportional, vertically projected area of vegetation (including leaves, stems, branches, etc.) above a given height. For this study, estimates of canopy cover were obtained on a near-annual basis from 1988 to 2016, from the Landsat sensor data. Otero et al. (2019) indicated that the Landsat-derived NDMI was sensitive to canopy cover and also better suited than the Normalized Difference Vegetation Index (NDVI) because of its greater dynamic range (approximately 0.65 compared with 0.28 for the NDVI). On this basis, Lucas et al. (2020) established a relationship between the NDMI and canopy cover (%), as determined from the Phantom-3 DJI RGB imagery, which was used to estimate canopy cover for each year from the single date or composite LANDSAT data (Figure 5a).

3.3.2 | Canopy height (m)

Based on acquisitions of DLR's interferometric Tandem-X (TDX) over the period 2011–2015, a CHM was generated for the MMFR mangroves (TDX_{CHM}; Lucas et al., 2020), with this corresponding through visual comparison to the LANDSAT NDMI image of June 15, 2015. The assumptions were made that the mean elevation of the underlying topography in the intertidal area was 0 m (mean sea level) and the slope was 0° (i.e., flat). The processing of the TanDEM-X Digital Surface Model (DEM) data to a ground resolution of 12.5 × 12.5 m was undertaken using the methods outlined in Wessel (2016) and is described in Lucas et al. (2020). The TDX_{CHM} was validated against eight CHMs retrieved from the 2020 DJI visible imagery acquired in 2016 (RMSE 1.94, R^2 = 0.89), which gave confidence in its use for quantifying canopy height across the MMFR. A CHM was also generated from the 2000 SRTM data ($SRTM_{CHM}$) using the approach of Simard et al. (2018) (Lucas et al., 2020).

3.3.3 | Vegetation lifeform, leaf type, phenology and stratification

The FAO LCCS differentiates lifeforms according to woody (trees and shrubs) and herbaceous (graminoids, forbs). Woody plants that are >5 m

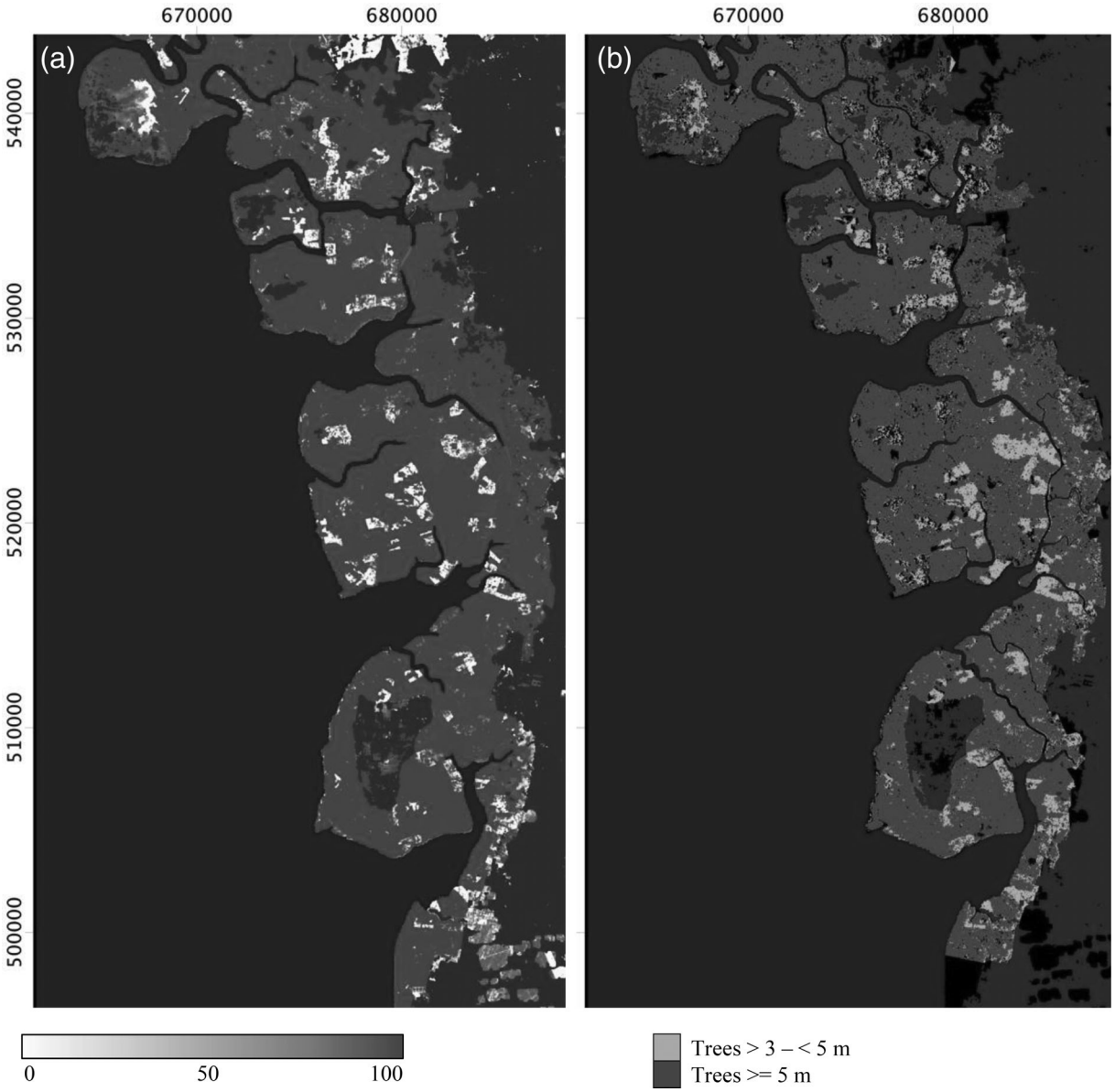

FIGURE 5 (a) Estimates of canopy cover (%) and (b) lifeform (physiognomic aspect of trees based on upper canopy height) generated for the MMFR, September 29, 2016. Coordinates are for Universal Transverse Mercator (UTM) Zone 47 N

are classified as trees. However, if the plant has a physiognomic aspect of a tree, then this threshold is lowered to >3 m (Di Gregorio, 2016). Mangrove lifeforms (trees) were defined on the basis of the height of the upper canopy and differentiated using thresholds of >3 to < 5 m and >=5 m, respectively so as to indicate early regrowth (Figure 5b). The former height range is generally associated with woody shrubs rather than trees, but woody plants with a physiognomic aspect of trees are classified as such if >3 m and < 5 m in height. Herbaceous vegetation was considered to be largely absent from the MMFR or occupying land parcels that were smaller in area than the 30 m pixel resolution of the Landsat sensor data. The leaf type and phenology descriptions were defined from knowledge, as all mangrove forests in the region are broadleaved and evergreen. Palms (mostly pinnate leaf type) and pine plantations (needle-leaved) were confined primarily to the terrestrial landscapes and were not included in the classification. Information on canopy layering was absent but managed forests were assumed to have one primary layer. The primary (virgin) forests are structurally diverse, as evidenced by the wider range of diameter densities reported by Otero et al. (2018), and hence can be considered as having at least two layers. However, quantitative measures of the height and cover of layers below the upper canopy (which can be described within the LCCS) were not available.

3.3.4 | Above-ground biomass (mg ha^{-1})

Although not used directly in the FAO LCCS, the above-ground biomass (AGB, Mg ha^{-1}) of mangroves within the MMFR, and based on the observation date of June 15, 2015, was estimated from the TDX_{CHM}. This was achieved by using a power relationship established by Fatoyinbo, Feliciano, Lagomasino, Lee, and Trettin (2017).

In Fatoyinbo, Simard, Washington-Allen, and Shugart (2008) the AGB for these plots was estimated using the allometric equations of Komiyama, Ong, and Poungparn (2008), which included measurements obtained originally from harvesting in the MMFR and tree diameter (D_{130}) as the dependent variable.

3.3.5 | Descriptors of non-vegetated land covers

All areas of estuarine and oceanic water were coded based on knowledge and according to their state (liquid), flow (moving), sediment loads (turbid in the near-shore environments) and inundation status (tidal), as dictated by the FAO LCCS taxonomy. Unconsolidated (fine grained) material was assumed on the exposed mudflats.

3.4 | Time extrapolation of biophysical variables

For each of the 98 dates of observation, the extent of clearance was associated with areas mapped as unvegetated in the LCCS Level 3 classification. By comparing maps of forest clearings generated using the thresholds of Landsat NDMI or $L_{HH}\sigma^o$ between July 29, 1988, (the first Landsat observation) and September 29, 2016 (the last ALOS-2 PALSAR-2 observation), time (in days) since clearing was estimated. The maximum age was 10,289 days (or 28.3 years) on September 29, 2016. An estimate of the time since clearing (in days) was then generated for each of the remaining 97 dates (Lucas et al., 2020), with only areas cleared since July 29, 1988 being considered. Significant changes were only observed on 68 dates, with this attributed, in part, to images acquisitions on proximal dates. The time in days was converted to forest age in years and months for ease of interpretation. Natural regeneration and/or direct planting (where necessary) was considered to occur from the date when the clearing was first detected.

Other areas in the productive zone of the MMFR were also at different stages of growth on the July 29, 1988 but were not able to be mapped because of similarities with mature forest in both the NDMI or $L_{HH}\sigma^o$. However, by assuming that all forests observed as being cleared were 30 years old at the time of clearance, their age was able to be estimated back in time and for one rotational cycle (to 1958). Whilst not directly used in this study, these estimates of forest age prior to each clearing event were included in the mapping so as to place the actual observed changes in the context of the previous logging and regrowth cycles.

Once established, the estimates of forest age provided a mechanism for estimating other EVs for each observation date. Estimates of canopy height were extrapolated to all 98 dates of observation using a non-linear relationship established between forest age (in 2015) and the TDX_{CHM} (Table 1—Equation 1; Figure 6a). These data were also used to generate a lifeform layer for each date that discriminated forest stands that were between >3 and < 5 m (early stages of regeneration) and >=5 m. The estimates of AGB derived from the TDX_{CHM} were used to establish a relationship with the age of forests on September 29, 2016 (Table 1—Equation 2; Figure 6b), which was then used to estimate the AGB for each of the 98 dates of observation and back to July 1988. LANDSAT sensor data were only available on an annual basis, either as single-date images or composites from multiple dates within the year. Thus, the canopy cover was assumed to remain constant within any 1 year unless a clearing event had occurred. On this basis, estimates of relative canopy cover (%) were generated for each year based on the LANDSAT-derived NDMI.

For each date of SAR observation only, and based on the clearing date, relative amounts of non-photosynthetic vegetation (NPV) in the form of woody debris (cut stumps and roots and branches: %) were inferred from the linear decline in the L_{HH} Digital Number (DN) from a maximum (approximately 7,000 DN or −6.1 dB) following clearing to a minimum (approximately 3,000 DN or −13.5 dB; Lucas et al., 2020). This decline takes place over a period of approximately 8 years but is reversed beyond this time because the wood debris has largely decomposed, and live trees regenerating or planted within the stand attain a size (and AGB) that is collectively sufficient to evoke double-bounce and subsequently volume scattering (Lucas et al., 2014, 2020; Table 1—Equation 3; Figure 6c). This transitional phase can be further described as the continued decline in L-band scattering beyond 5–6 years since clearing (associated with decomposition of larger woody elements) is mirrored by an increase in the NDMI. The cross-over between these two measures indicates when the wood debris is overtopped by the increasing amount of foliage in the canopy (Lucas

TABLE 1 Relationships describing the trends in biophysical variables with age

No.	Equation	y	x	R^2	n
1	$y = -0.015(x^2) + 1.1412x^4$	[c]CHM (m)	[a]Age (years)	0.92	331
2	$y = 91.369\ln(x) - 95.839$	[c,d]AGB (Mg ha^{-1})	Age (years)	0.88	166
3	$y = -0.0187x + 146.17$	[d]L_{HH} DN	% Decomp	0.74	292

[a]RMSE of 1.94 m in estimation of canopy height from TanDEM-X when compared with CHMs generated from DJI Phantom RGB images (Lucas et al., 2020).
[b]Typical errors in the estimation age ± 6 months for all age classes (Lucas et al., 2020).
[c]RMSE of 148 Mg ha^{-1} for SRTM-retrieved AGB based on Simard et al. (2018), RSME of 79 Mg ha^{-1} based on comparison with ground data from the MMFR.
[d]For forests older than 3 years.
[e]Indicates relative amounts of woody debris amounts.

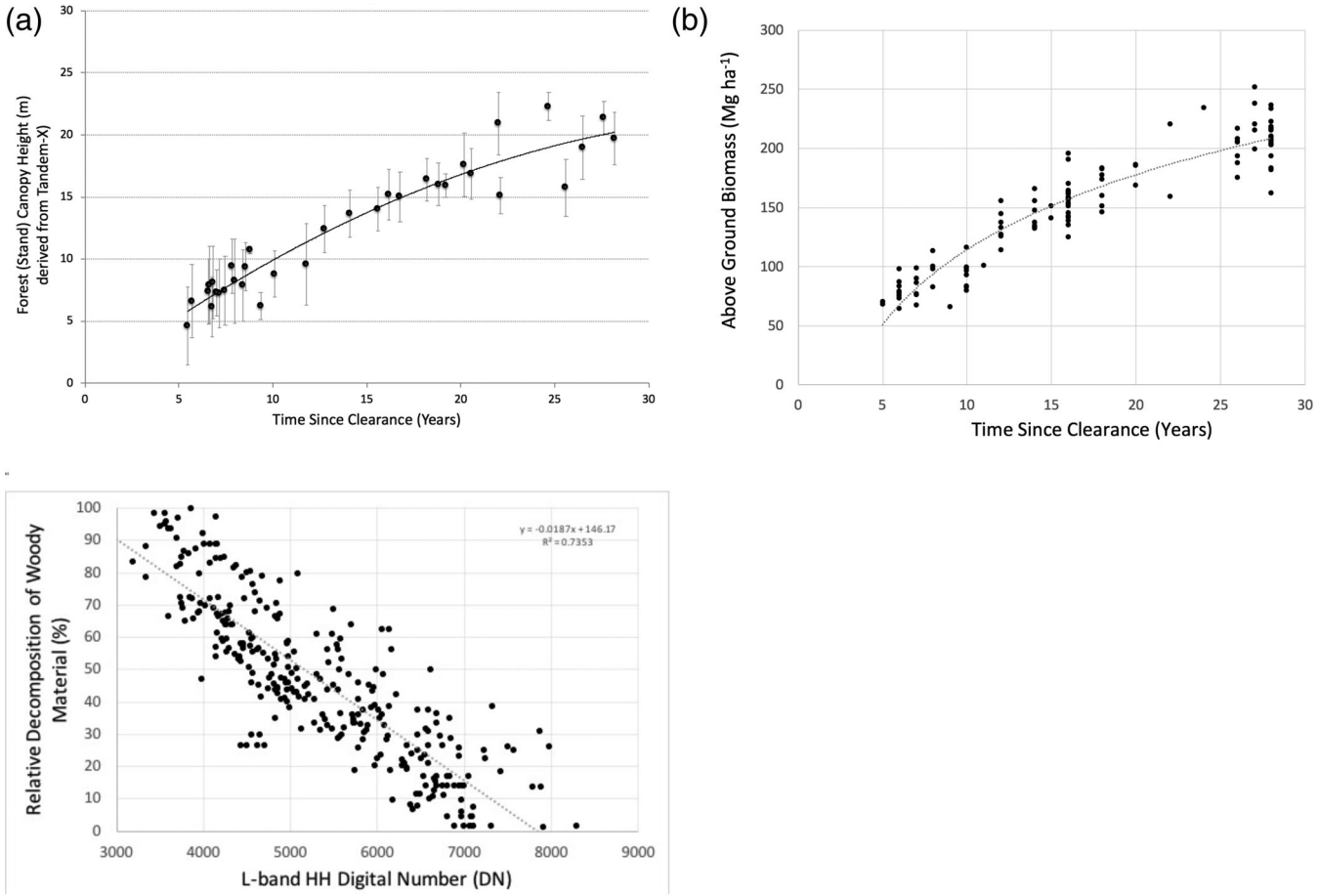

FIGURE 6 Observed (a) increase in above-ground biomass (Mg ha^{-1}; derived from the TX_{CHM}), (b) decrease in LHH (DN) following clearance of mature production forests, and (c) Relationship between L-band HH (Digital number DN) and the relative decomposition of woody material (%)

et al., 2020; Otero et al., 2019). However, this debris is still detected at L-band HH, in particular, because of penetration of microwaves through the foliage and smaller branches of this canopy. Thus, the trends in L_{HH} and NDMI provide a unique insight into the nature and timing of the processes of decomposition and regeneration occurring in the first decade following clearing.

Using the framework of the Level 3 classifications for each observation date, more detailed descriptions to Level 4 were generated using EDs associated primarily with the vegetation and water categories listed within the FAO LCCS taxonomy but also those that were external (namely AGB and NPV). The resulting map legends together with the component and cumulated codes and their translation to descriptive text were stored within the RAT for each date.

3.5 | Classifications of land cover change (1988–2016)

By comparing (a) the LCCS Level 3 categories, (b) LCCS Level 4 component codes (e.g., B6 to B5; 3–7 m to 7–12 m in height) and, c) EDs external to the taxonomy (e.g., AGB, NPV) between any two time-separated periods (available for each observation date) and referring also to the pre-change and post-change states and conditions, evidence-based change maps were generated. This approach, described originally by Lucas and Mitchell (2017), defines change categories *a priori* and identifies and selects layers that might provide evidence for these changes. Descriptions of these changes are then based on the cumulation of this information. The main target categories demonstrated in this study were clearing (i.e., logging) and regrowth.

4 | RESULTS

4.1 | Temporal estimation of EDs

The comparison of maps of forest age over the 28-year period (since July 1988 and 2 years short of a full 30-year rotation) highlighted the progressive logging of forests as they matured and subsequent ageing of naturally regenerating and/or planted forests within each coupe. Examples of these are given in Figure 7a, whereby the increasing age of forests following clearing events is tracked. Subsets of height and AGB estimates for these same dates, and estimated from age, are given in Figure 7b,c, respectively, and convey the vertical development of the canopy and accumulation of above-ground carbon by the forests over time. Temporal information on changes in tree growth stage (lifeform) was also generated from the height information and the

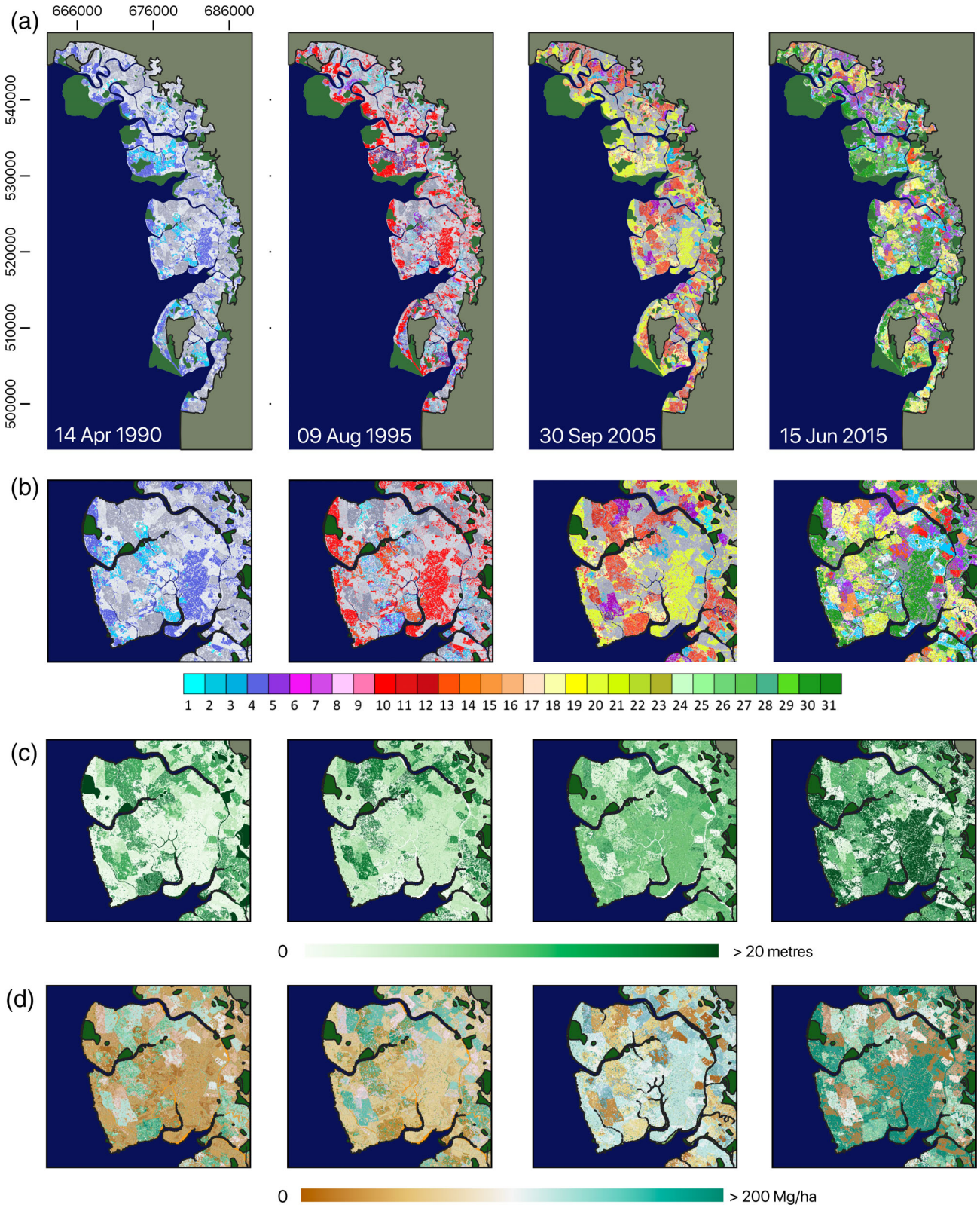

FIGURE 7 Example temporal maps of EDs generated for the MMFR. (a) and (b) Forest age in years, (c) canopy height (m) and (d) above-ground biomass (Mg ha^{-1}) for four selected years [Colour figure can be viewed at wileyonlinelibrary.com]

decomposition of woody material was inferred from the L-band SAR data. Prior to the dates when clearances were detected, the age of forests was backdated for each time-step by assuming that these had been cleared when they had reached 30 years of age. Within the 318.1 km^2 for which the age of forests was estimated from the time-series of satellite sensor data and for the productive zone, 258 km^2

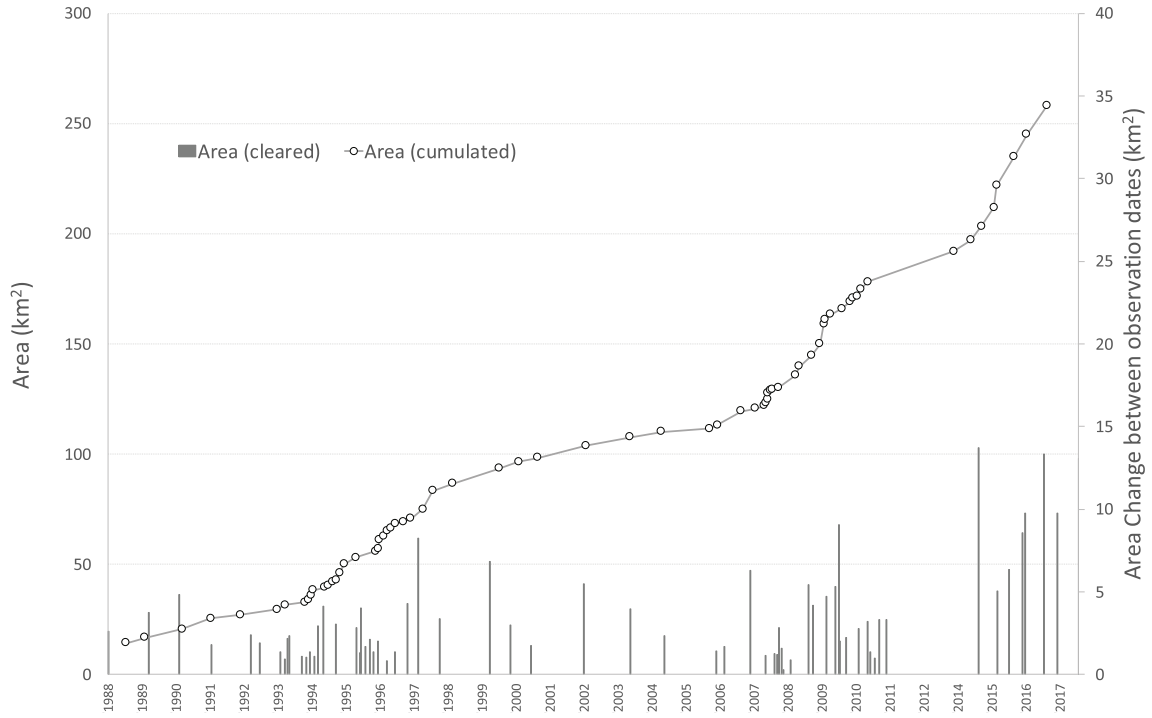

FIGURE 8 Progressive increase in the area of mangrove forest cleared in the productive zone and the rates of change between different observation times

was cleared from 29th July to September 29, 2016 (Figure 8). The rates of clearing between dates varied over the time-series but generally averaged about 3.79 km^2 (range 0.28–14.1 km^2). Rates of clearing were comparatively high from 2014 onwards. The greater frequency of observations during the acquisitions of L-band SAR data provided more information on the clearing rates and patterns.

4.2 | Land cover classifications from variables

Land cover classifications were generated for the MMFR for each of the 98 observation dates and according to the FAO LCCS Level 4 taxonomy. Examples are illustrated in Figure 9 (for July 30, 2000, and September 29, 2016), with each constructed from a range of EDs used directly within the LCCS taxonomy. Each land cover description was augmented with additional information external to the FAO LCCS taxonomy (e.g., AGB, woody debris and also age). As EDs are consistently retrieved for each date, comparisons can be undertaken for any two time-separated points and used to highlight changes that have occurred historically.

The LCCS legend for each pixel was stored within the KEA RAT, with this allowing export to shapefiles for any time step through PYTHON scripts. This collation of different EDs derived from satellite sensors observing in different modes (e.g., optical, single and dual polarisation and interferometric SAR) provided a mechanism by which to collectively describe and summarise the structural composition and complexity of the mangrove forests as well as the characteristics of the non-forested areas, including recent clearances.

The accuracy of the classification is dependent upon that of the ED layers used as input, with these indicated in Lucas et al. (2020) and Table 1. However, a further indication of accuracy was obtained by comparing the estimates of canopy height for 2000 obtained (a) by applying the relationship established between the TDX_{CHM} and forest age (for 2015) to the age class map for 2000 and (b) from the $SRTM_{CHM}$ (Figure 10). The map comparison indicated a close correspondence in both the distribution of logged coupes, noting that the SRTM data were not used for the generation of the forest age maps, and also in the spatial distribution of forests within different height ranges. The close correspondence was also confirmed by comparing estimates extracted from 438 polygons of between 1 ha and 1 km^2 in area and located over relatively homogeneous forests of varying age (RMSE = 5.28 m). Greater homogeneity in the distribution of height retrieved from the age class map was observed when compared with the more direct measures from the SRTM, with this resulting from the formation of segments of similar age within the time-series of Landsat and L-band SAR data.

4.3 | Changes in LCCS categories and EVs

Changes between major land cover were first identified by comparing the Level 3 classes between two periods, and where these differed,

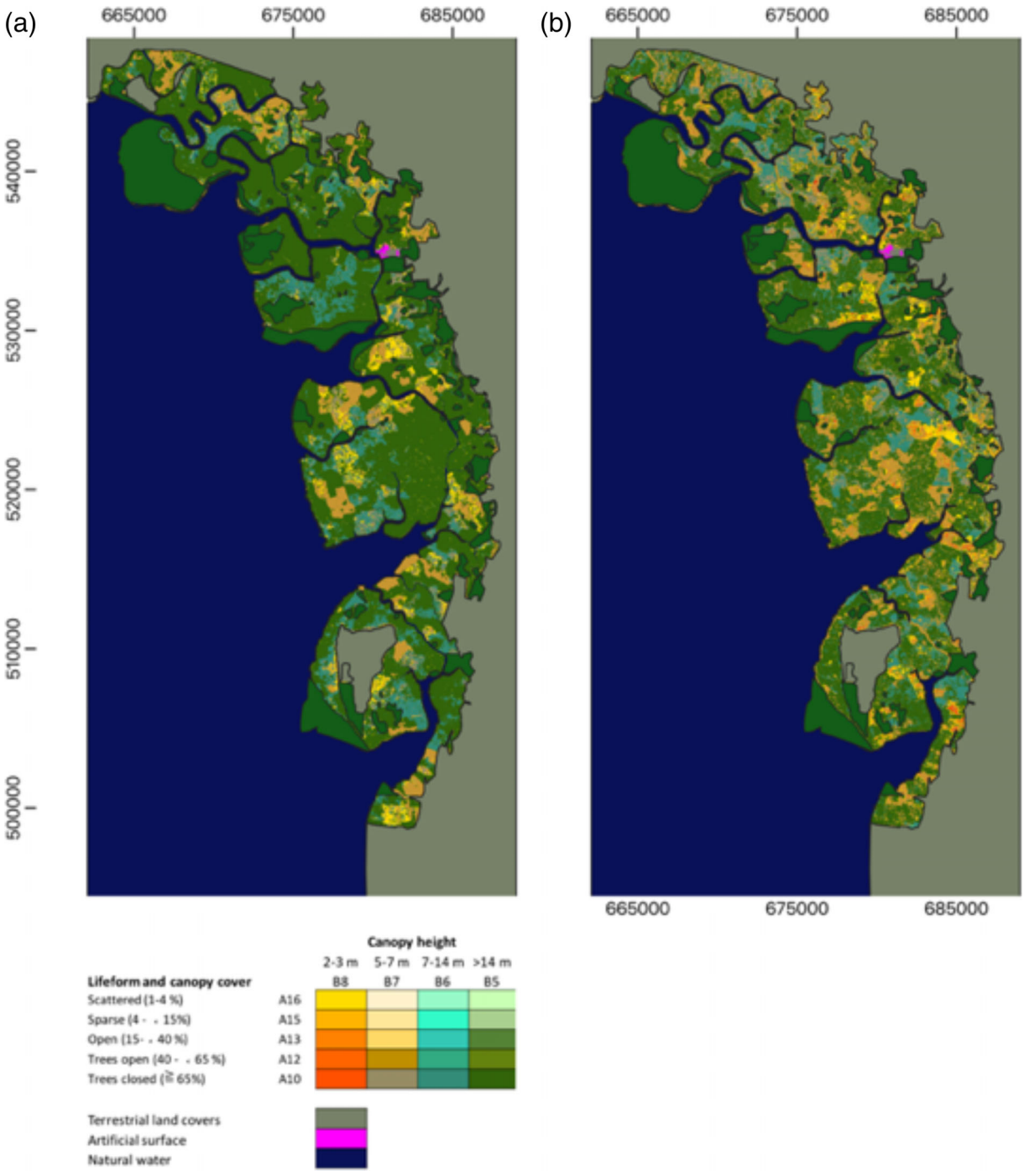

FIGURE 9 LCCS Level 4 classifications of the MMFR for (a) July 30, 2000 and (b) September 29, 2016. Each image is associated with a Raster Attribute Table (RAT) that contains information on mangrove forest age (days or years since clearing), AGB (Mg ha^{-1}), canopy cover (%) and height (m) and lifeform. Additional information on, for example, the amounts of woody debris (relative %), dominant plant species, water states, movement and turbidity, can be included [Colour figure can be viewed at wileyonlinelibrary.com]

major transitions in the extent of broad land covers were indicated. An example (Figure 11a) is the change from aquatic natural/semi-natural vegetation (comprised of mangroves) to naturally bare surfaces and vice versa. In these cases, information on the states of both categories prior to and following changes can be obtained through reference to the Level 4 categories and EDs external to the LCCS. Where the Level 3 classes remained the same, however, the FAO LCCS component codes at Level 4 (e.g., relating to canopy cover and height) and EDs external to the LCCS (e.g., AGB) provided information on changes in condition (Figure 11b). Note that both canopy height and AGB were derived from forest age. This information was then collectively cumulated between the two time periods to allow mapping and more comprehensive descriptions of the two pre-defined change categories of clear cutting (logging) and regrowth

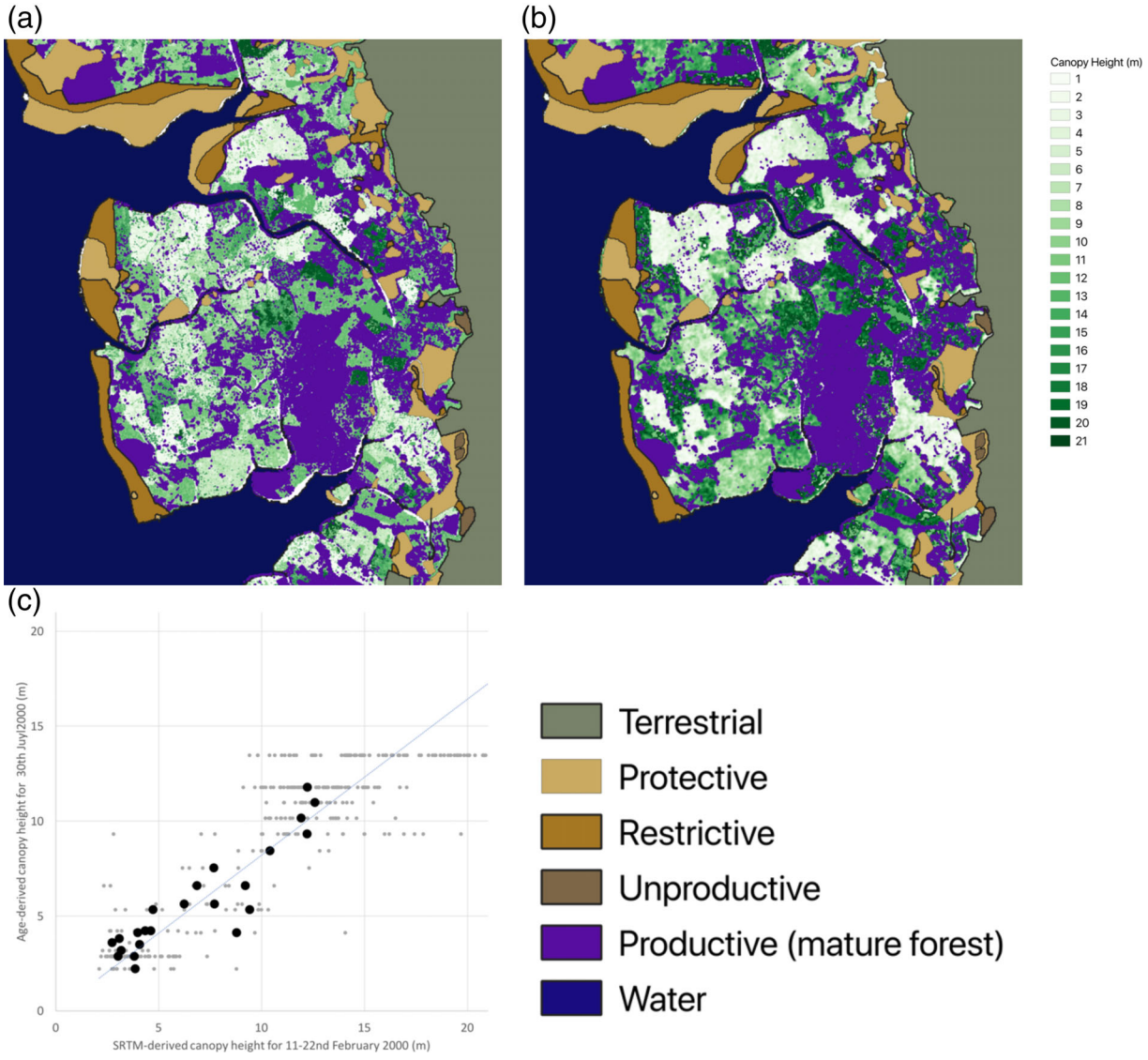

FIGURE 10 Canopy height estimated for 2000 from (a) age (estimated for July 30, 2000) and (b) SRTM data acquired between February 11 and 22, 2000. (c) Comparison of estimates for different age bins of 1 year (RMSE = 5.28 m, n = 438) [Colour figure can be viewed at wileyonlinelibrary.com]

(Figure 11c). Logging, as an example, was linked to a Level 3 change from natural/semi-natural aquatic vegetation (mangrove) to a bare surface but also a total loss of canopy cover and height. Regrowth was conversely identified initially as a transition from a naturally bare surface to natural/semi-natural aquatic vegetation. This was linked to the removal and decomposition of woody debris, which was evidenced by a progressive reduction in $L_{HH}\sigma^{o}$ followed by progressive increases in canopy cover, and obscuration of the forest floor and remaining debris, as well as height and AGB and transitions between lifeform classes (trees >3–5 to 5 m to >5 m). Thinning of the productive forests typically occurs at 15 and 20 years, but this was unable to be reliably detected from the available remote sensing data. The changes identified were again stored internally within the RAT as were transitions within EDs (e.g., age, AGB and relative amounts of woody debris).

5 | DISCUSSION

5.1 | Use of EDs for land cover classification

Exploiting EDs to generate land cover and change classifications based on the FAO LCCS taxonomy and within the framework of EODESM provides a robust, reproducible, flexible and understandable approach to establishing the status and monitoring mangroves in the MMFR. The nominal 30-year rotation logging cycle and rapid growth rates of mangroves provided a dynamic landscape to evaluate this approach. Of note is that retrievals and associated classifications can be undertaken at any spatial scale and for different points in time, provided relevant data are available.

This study has specifically demonstrated how optical, L-band SAR and interferometric SAR can be used for ED retrieval. However,

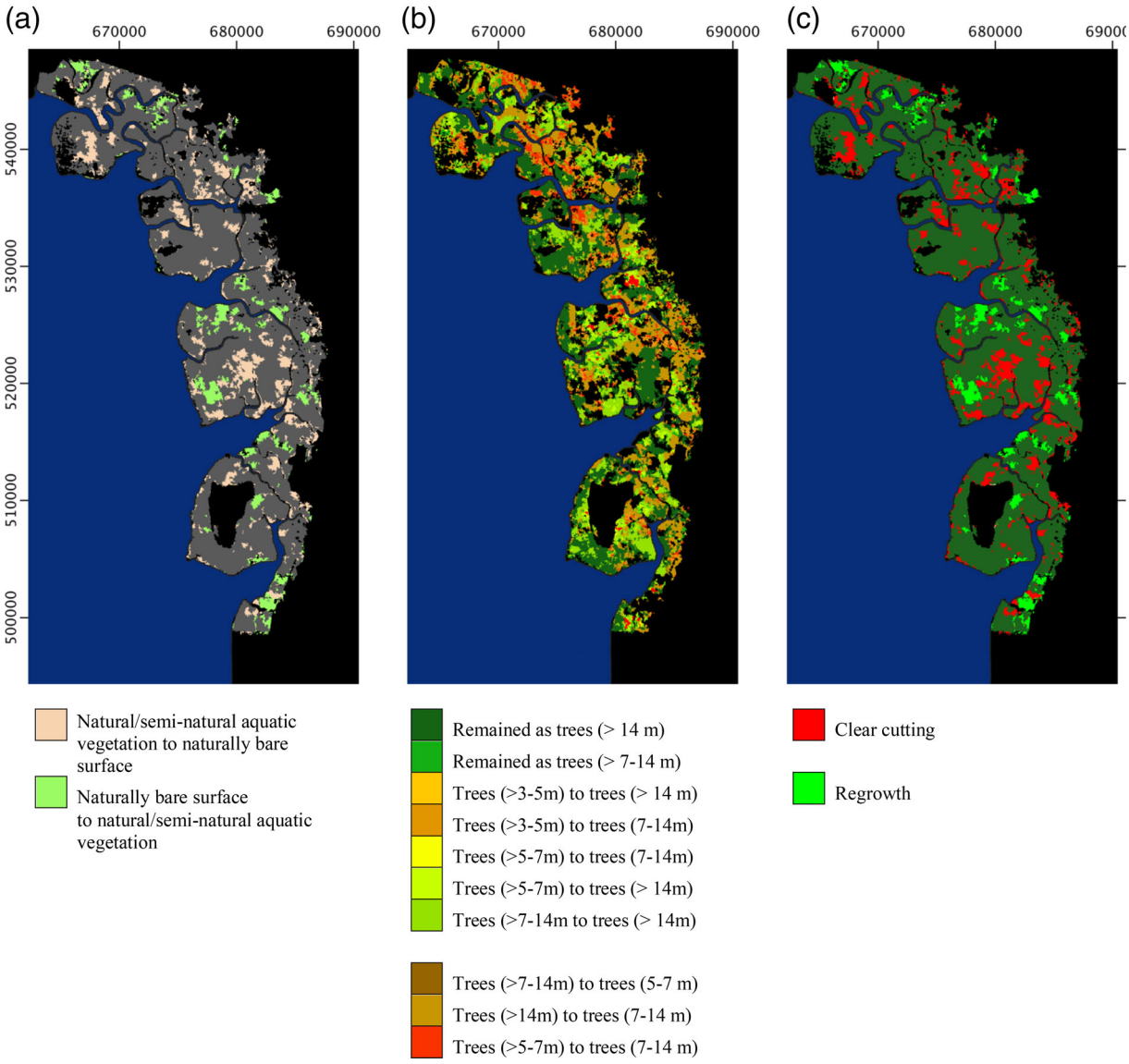

FIGURE 11 Changes (a) between LCCS Level 3 categories (natural aquatic vegetation [i.e., mangroves] and bare surfaces) and (b) within LCCS 4 category canopy height classes (defined by the FAO LCCS). Note that a height value is not associated with regrowth in 2016 as this is a between class change. Some forests have also been cut and have subsequently regrown between the two dates. The products are generated from a comparison of classifications for July 30, 2000, and September 29, 2016. Areas that have been clear cut on or just before September 29, 2016 and regrowing on areas that were identified as cleared on July 30, 2000 are highlighted. All image products are projected to Universal Transverse Mercator (UTM) Zone 47 North [Colour figure can be viewed at wileyonlinelibrary.com]

EODESM allows integration of a wide range of EDs for classification and description, and these can be retrieved from any sensor operating in appropriate and relevant modes and for which algorithms exist for retrieval or can be developed. This is because the classifications of land cover and change and associated descriptions are based on the integration of EDs with defined codes or units. As such, the approach is applicable to landscapes globally. The retrieval of EDs and associated classifications of land cover and change is also scale independent. As an example, classifications can be generated from very high (<2 m) imagery, such as the WORLDVIEW-2 optical sensor and airborne (including drone) datasets. The use of WORLDVIEW-2 is advantageous as it offers stereo capability and potential to retrieve canopy height (Lucas et al., 2020). These data can also provide more detailed information on tree and forest dynamics, including dominant tree species compositions, although their current cost may be prohibitive. Land covers and change in the landscape proximal to the MMFR were not mapped as EDs were unable to be reliably retrieved, primarily because of the lack of supportive ground data. However, EODESM is considered to be particularly suitable for application to other land covers and also mangrove areas that might be subject to management in future years.

Estimation of forest age was an essential component of the temporal classifications as other attributes (e.g., canopy height, AGB and lifeform) depended on relationships with this variable. With a nominal

30-year rotation cycle, the estimation of age requires the use of LANDSAT sensor data as these have been acquired since the mid-1980s. Annual observations are generally sufficient for mapping, given that clearances remain evident within both LANDSAT and L-band SAR data for up to 8 years after the clearing event and regrowth following natural colonisation or replanting is progressive as forests mature. However, the integration of L-band SAR or higher frequency optical (including Sentinel-2) data for selected periods provides an opportunity to obtain more detailed information on the location and timing of logging and insight into the formation of logging coupes (Lucas et al., 2020). L-band SAR data are particularly useful given capacity for data acquisitions regardless of weather and illumination conditions and a recommendation is that such observations be used to capture sub-annual observations of change, with a 6-month repeat considered sufficient. In the future, L-band sensors such as the ALOS-4 PALSAR-4 and the NASA-ISRO Synthetic Aperture RADAR (NISAR) will provide new datasets that will support ongoing monitoring of mangroves in the MMFR and hence early adoption of these data would be beneficial. These data provide greater capacity for mapping clearances compared to C-band SAR, which provide less discrimination between vegetated and unvegetated areas and lifeforms.

Canopy height was able to be retrieved from the TanDEM-X interferometric SAR data and AGB could be inferred from these data. The use of age information to infer structural attributes (namely canopy height and AGB) over extended periods was essential, given the restricted acquisition times of interferometric SAR data. This is also unavoidable, given that some variables (e.g., canopy height) are not able to be retrieved on a frequent basis because of the lack of satellite sensors operating in specific modes (in this case, interferometric SAR). However, the close correspondence with the height retrieved from the SRTM indicated that the use of age information provided a viable approach for retrieving the height of mangroves that are under rotational management. Natural variations in height and AGB may nevertheless occur because of adverse or favourable growth conditions, such as prolonged inundation or changes in nutrient input, which can lead to errors when these EDs are estimated from age alone. This was highlighted in the comparative study of Otero et al. (2020), which indicated variable recovery in different forest stands as a function of location (e.g., distance to water). Other sources of height information could also be integrated to inform on the dynamics of mangroves and to validate height or AGB maps derived from age. These include data from the ICESAT-2 and the Global Ecosystem Dynamics Investigation (GEDI; both launched in 2018), which could be exploited in future years. For canopy cover, and as with many EDs requiring optical data for retrieval, sub-annual estimates were difficult to obtain from the Landsat NDMI because of cloud cover in many scenes and hence the classification within years needed to refer to the single date imagery or annual cloud-free composites.

Many studies have advocated the use of L-band SAR backscatter, and particularly $L_{HV}\sigma^{o}$, for retrieving the AGB of woody vegetation because of the asymptotic increase with AGB up to approximately 60–100 Mg ha^{-1} (e.g., Hamdan, Aziz, & Hasmadi, 2014; Luckman, Baker, Honzak, & Lucas, 1998). However, within the MMFR, both $L_{HH}\sigma^{o}$ and $L_{HV}\sigma^{o}$ fluctuated over the 30-year rotational cycle (Lucas et al., 2020), which compromised retrieval of AGB from these data. A further limitation of using Japanese L-band data is that the archive omits the periods pre-1992, 1999–2006 and 2011–2014, which prevents estimation of AGB but also the retrieval of relative amounts of woody debris from SAR outside of these periods. The LANDSAT sensors have been acquiring data every 16 days since the mid-1980s to the present day and can, therefore, be used to fill gaps in the L-band SAR temporal coverage and allow better estimation of forest age. Woody debris is less able to be detected from LANDSAT sensor data and hence such information cannot be obtained without the use of L-band SAR.

The FAO LCCS does not consider plant species but the EODESM system allows for such information to be included as an additional descriptor of the land cover classes. However, mangrove species were difficult to discriminate from the LANDSAT sensor data, largely because differences in structural development led to a high level of variability in near infrared (NIR) and shortwave infrared (SWIR) reflectance within and between forests with different species dominance and over time. The majority of mangroves in the productive zone were dominated by *R. apiculata* and *R. mucronata* with other species being less prevalent. The exception was along the coastal margins, where historically (and also today) mangroves have been dominated by *Avicennia–Sonneratia* species (Ariffin & Mustafa, 2013). Whilst some spectral differences in forests dominated by these different species were evident, particularly within the red edge and NIR WORLDVIEW-2 data, these were insufficient to allow discrimination from the LANDSAT sensor data (which lacks a red edge channel). However, it was noted that early regrowth forests of lower stature and dominated by *Rhizophora* species identified in the DJI Phantom RGB imagery were spectrally similar in the WORLDVIEW-2 red edge and NIR data to taller (e.g., > 10 m) *Bruguiera* species, but became more distinguishable over time. Thus, the combination of reflectance and canopy height data might provide a future avenue for discrimination of several dominant species in the MMFR. Further information on non-vegetated land covers (e.g., water, bare surfaces) can be included within the LCCS classification (e.g., tidal extent, water flows and sediment loads), but spatial datasets representing these were not available for this study and were necessarily based on knowledge.

5.2 | Detecting change

The integration of the component land cover classes and EDs for generating evidence-based change mapping represents a powerful approach to fully quantifying and understanding the cycles of management within the MMFR. Four broad stages within the rotation can be described both from the ground and from remote sensing data (Figure 12). Whilst several of the EDs can be retrieved or estimated directly from the satellite sensor data (e.g., canopy cover, height, AGB, relative amounts of woody debris), knowledge can also be incorporated into EODESM. For example, mangroves are broadleaved (Goessens et al., 2014; Otero et al., 2018), typically evergreen (with

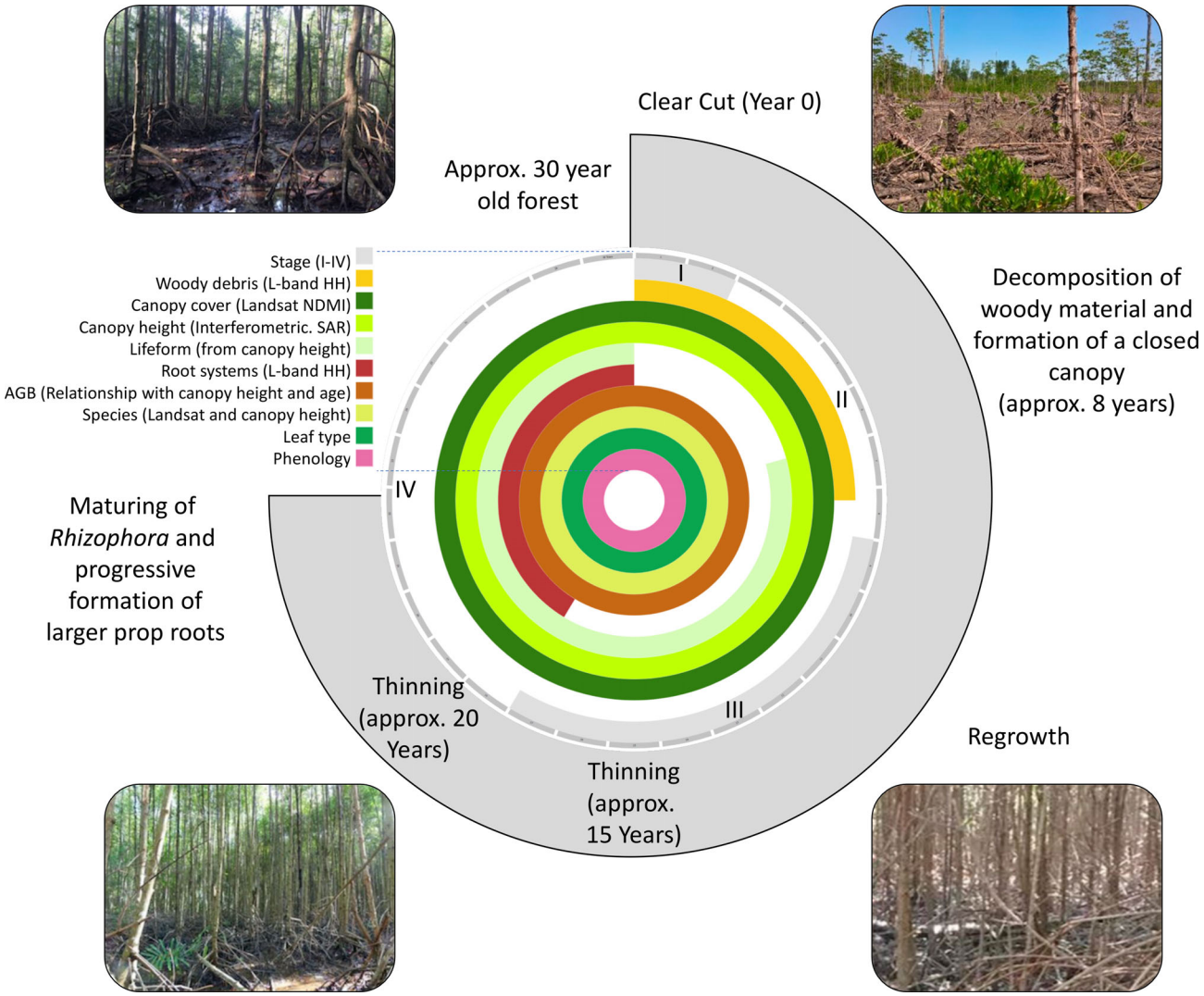

FIGURE 12 An overview of a typical logging cycle, which takes place over approximately 30 years, and its description using combinations of EDs retrieved from different sources (satellite sensors operating in different modes, knowledge). The sequence considers clear felling (Stage I, which takes up to 2 years for each coupe), decomposition of woody debris and formation of a closed canopy (II), maturing of the forest (including thinning; III) and formation of substantive prop root systems (IV) in the *Rhizophora*-dominated forest (Lucas et al., 2019) [Colour figure can be viewed at wileyonlinelibrary.com]

some exceptions; Pastor-Guzman et al., 2018) and tidally inundated. Many of the changes occur concurrently, including the decomposition of woody material and the progressive structural development of forests and accumulation of AGB, which facilitates mapping of several change events or processes.

Evidence of clearing, which can take place over a period of up to 2 years for each coupe, includes a sudden loss of canopy cover (%) and forest height (m) as trees are felled and the wood debris (non-photosynthetic material (%) remaining as cut stumps and discarded branches) leads initially to a rapid increase in L-band backscatter, particularly at HH polarisations. As the wood debris decomposes or is removed through the tidal movement of water, the $L_{HH}\sigma^{o}$ also progressively decreases to a minimum, with this assumed to be linear. The NDMI conversely reflects the increase in canopy cover which reaches full (approximately 100%) vegetation cover after about 5.9 years on average (Otero et al., 2019). However, the high $L_{HH}\sigma^{o}$ indicates that woody debris is still present, although it is shielded from view by the closed canopy cover. Once a full canopy is established, an increase in both $L_{HH}\sigma^{o}$ and $L_{HV}\sigma^{o}$ is observed as the individual trees increase in size (diameter and height) and transition from trees (3–5 m) to trees (≥5 m in height), with this reflecting the progressive accumulation of biomass (Mg ha^{-1}) within the wood associated with an increase in canopy cover and height. Thinning of the forests is best indicated by a decrease in canopy cover at approximately 20 years, although this is difficult to discern from optical or SAR data. The forests attain their maximum height and cover at about 30 years of age, after which felling again takes place and the cycle is repeated.

To better identify the two time steps between which comparisons in LCCS codes and EDs are most useful, change detection algorithms can be used with candidates being cross correlation analysis (Tarantino,

Adamo, Lucas, & Blonda, 2016) and the Breaks For Additive Season and Trend (BFAST; Verbesselt, Hyndman, Newnham, & Culvenor, 2010). For the MMFR, such methods could be adopted to routinely detect the timings of clear cutting and hence when to also target EO data for describing the pre and post clearing conditions within the 30-year growth cycle. The time since clearing, and hence the age of forests, can also be quantified with each new image acquisition. Similarly, these data can be used to track the progression of forest structural development and AGB accumulation and turnover. Time-series comparison of descriptions from the two identified time stamps discerns the nature of change events or processes (e.g., deforestation, decomposition of woody debris, attainment of full canopy cover, growth and thinning) based on evidence, which is a common requirement for management. Classifications are able to be easily updated as and when new imagery are acquired and using EDs retrieved directly or inferred from the relationships with forest age. Furthermore, as knowledge of the age of forests is known, several EDs (including height and AGB) can be predicted at least to the end of the current rotation and hindcasting of the states of the forest can also be undertaken, as demonstrated in this study. EODESM, therefore, provides a framework that can facilitate ongoing robust and consistent monitoring of the MMFR to better support sustainable use and management.

5.3 | Implications for management

EODESM provides a new approach to ongoing monitoring, historical referencing and prediction of EDs and land covers that is applicable to the MMFR but also other mangrove sites either under similar management or where this is proposed in the future. The rotational cycle of timber harvesting, regrowth and maturing were tracked and described using an evidence-based approach that integrated EDs retrieved or extrapolated from optical, X-band interferometric SAR and L-band SAR data. This study, which builds on Lucas et al. (2020), provides key relationships between EDs and forest age that can be applied each time a new image is acquired with these then used to update the mapping. The EO data that allow updates are currently freely available and include the LANDSAT but also SENTINEL-2 optical sensors, although observations from these may be limited by persistent cloud. For this reason, currently operating (ALOS-2 PALSAR-2) and future L-band SAR are recommended, as these provide the cloud-free observations needed to detect clearances and also have sensitivity to relative amounts of woody debris.

The approach developed is based on 10 or 30 m spatial resolution data and hence detailed information on forest dynamics (e.g., succession during different growth phases, dieback and degradation through lightning strikes) are not able to be easily discerned. This requires the use of higher spatial resolution (primarily optical and/or LIDAR) spaceborne and airborne data. This is recommended given the additional information obtained on the states and dynamics of mangroves, whether in rotational management or in protective reserves. Tracking the rotational cycle through integration of satellite-derived EDs provides forest managers with a quantitative and transferable approach for describing the state and condition of the productive mangrove zones for any point in time. However, further validation of EDs retrieved from the EO data and also derived maps of land cover and change is recommended, including through the use of mobile applications and drones. Of note is that the classifications can be improved by simply replacing refined estimates of EDs with those used in this study if these are proven to be more robust. Thus, EODESM offers the potential for continuous improvement in monitoring capability as new information is obtained. Quantitative information on other EDs (e.g., species, water related), including in the adjoining terrestrial landscapes, could also be obtained in order to refine and extend the land cover classifications.

EODESM also has potential application for detecting change in unmanaged and natural mangroves. For example, quantitative (areal extent) and qualitative (plant species composition and functional) degradation of land covers can be detected, as well as change processes. These might include identifying conversions (whether legal or illegal) of mangroves into other land uses (Richards & Friess, 2016), pinpointing selective cutting in unmanaged forests (Hirschmugl, Steinegger, Gallaun, & Schardt, 2014), or detecting cryptic ecological degradation (Dahdouh-Guebas et al., 2005). As with existing or planned managed areas, this could be achieved by exploiting the same satellite sensor data used in this study, with this ideally supported by ground-based or aerial (including drone) measurements or observations and undertaken as part of a multi-scale strategy. The approach also has considerable potential for planning and/or monitoring programmess aimed at restoring mangroves, including in Southeast Asia (Ilman, Dargusch, & Dart, 2016; Proisy et al., 2018).

The estimates of forest age are based only on those coupes that have been cleared since the commencement of Landsat acquisitions and their availability. However, the rotational cycle of production for the MMFR is 30 years and so it was assumed that when forests were cleared, they were this age. On this basis, their age in preceding years was able to be estimated back to 1958 but this could be extended to the start of the logging activities if the rotational cycle was adhered to. However, this needs to be evaluated against the earliest records of logging from the MMFR, which is the subject of ongoing research. Similarly, future predictions of forest age and also canopy height and AGB can be made, which can assist management planning.

Whilst the approach has been applied to commercially managed mangroves, it is also relevant for describing the progression in natural settings, although forest age can only realistically be quantified where observations prior to colonisation are available. For forests growing prior to 1985, ageing forests is difficult from the LANDSAT series as data were only captured from this year. However, reference could be made to, for example, pre-1985 LANDSAT Multispectral Scanner System (MSS) data or aerial photography.

6 | CONCLUSIONS

The study has established that EODESM provides a robust framework for quantifying current, past and future dynamics of the commercially harvested mangroves of the MMFR. Descriptors of mangroves through

their rotational cycle were obtained at least annually for the MMFR between 1988 and 2016 from quantitative measures of EDs retrieved from time-series of optical and radar satellite sensor data. Of these, canopy cover was retrieved directly from theLANDSAT NDMI, forest age was determined from observations of clear felling during the observation period, and canopy height was estimated based on a relationship established with forest age and the 2015 TanDEM-X CHM. AGB was estimated from canopy height and extrapolated through the time-series using relationships with age. On the assumption that forests are managed on a 30-year rotation, the age of forests and associated estimates of EDs were estimated prior to 1988 and beyond 2016. The close correspondence between canopy heights estimated indirectly from forest age and directly from the SRTM for 2000 confirmed reliable estimation of age and associated EDs from the EO datasets. From the range of EDs retreived or estimated, land cover classifications were generated using EODESM and according to the FAO LCCS taxonomy. Comparison of the resulting land cover components (e.g., mangrove lifeform, canopy height and cover) and additional descriptors (AGB, age, woody debris) allowed evidence of pre-defined change events (i.e., cutting) and processes (decomposition and removal of woody debris, forest growth) to be gathered, with this assisting mapping of these processes.

Whilst EODESM has been applied to medium resolution imagery, it can be applied at any scale because of its use of EDs with unit measures (i.e., time, m, Mg ha^{-1}, %). This opens opportunities for use athigher spatial resolution and over a range of mangrove situations. Multi-scale comparison of data acquired, including at the ground level and from drones, can also be used for validation purposes. The advantage of the approach is that EDs, generated using different algorithms, can be substituted into the classification. In the immediate future, integration of the Sentinel-2 optical and L-band SAR is recommended, given their sensitivity to a range of EDs, including those relating to the foliar and woody components of vegetation.

EODESM has potential to assess the sustainability of production and assist future planning and management as well as conservation activities. As EODESM relies entirely on EDs retrieved from satellite sensor data, there is considerable potential for its application in other mangrove regions within and outside of Malaysia and is recommended for some areas where logging is ongoing or proposed.

ACKNOWLEDGEMENTS

This research was funded by BELSPO (Belgian Science Policy Office) in the frame of the STEREO III Programme—Project Managing Mangrove Forests with Optical and Radar Environmental Satellites (MAMAFOREST) grant number SR/00/323. We thank the Steering Committee members Marc Simard (NASA-JPL), Tiejun Wang (Universiteit Twente) and Daniel Friess (National University of Singapore) for their independent assessments and Joost Vandenabeele and Jean-Christophe Schyns for Belspo STEREO III Programme Management. We also thank the Perak State Forestry Department and the local rangers of the MMFR for their support during the fieldwork and for providing the management plans of the reserve. Finally, we thank Muhammad Amir Bin Fisol, Emilia Ashari and Columba Martínez-Espinosa, for their collaboration with field work. This study was carried with the approval of the Perak State Forestry Department, Ipoh, Malaysia. LANDSAT Surface Reflectance products courtesy of the US Geological Survey. The authors would also like to thank both the University of New South Wales and the European Regional Development Fund (ERDF) Sêr Cymru programme for providing support to R. Lucas. The Japan Aerospace Exploration Agency (JAXA) Kyoto & Carbon Initiative are thanked for providing the L-band SAR data for the study as are members of the EU's BIOSOS and Ecopotential Projects, the Aberystwyth University Living Wales Team and Geoscience Australia.

AUTHOR CONTRIBUTIONS

The MAMAForest Project Team (Lucas, Otero, Van De Kerchove, Dahdouh-Guebas and Satyanarayana) conceptualised the research and contributed towards the analysis and interpretation of the EO datasets. The analysis of the interferometric SAR data was undertaken in conjunction with Lagomasino and Fatoyinbo.

ORCID

Richard Lucas https://orcid.org/0000-0003-3010-3302
Temilola Fatoyinbo https://orcid.org/0000-0002-1130-6748

REFERENCES

Alongi, D. M. (2008). Mangrove forests: Resilience, protection from tsunamis, and responses to global climate change. *Estuarine, Coastal and Shelf Science*, *76*, 1–13. https://doi.org/10.1016/j.ecss.2007.08.024

Alongi, D. M. (2012). Carbon sequestration in mangrove forests. *Carbon Management*, *3*, 313–322. https://doi.org/10.4155/cmt.12.20

Ariffin, R., & Mustafa, N. M. S. N. (2013). *A working plan for the Matang Mangrove Forest Reserve, Perak* (6th revision ed.). Ipoh, Malaysia: State Forestry Department of Perak.

Ashton, E. C., Hogarth, P. J., & Ormond, R. (1999). Breakdown of mangrove leaf litter in a managed mangrove forest in Peninsular Malaysia. *Hydrobiologia*, *413*, 77–88. https://doi.org/10.1023/A:1003842910811

Azahar, M., & Nik Mohd Shah, N. M. (2003). *A working plan for the Matang Mangrove Forest Reserve, Perak: The third 10-year period (2000-2009) of the second rotation* (Fifth revision). Ipoh, Malaysia: State Forestry Department.

Aziz, A. A., Phinn, S., Dargusch, P., Omar, H., & Arjasakusuma, S. (2015). Assessing the potential applications of Landsat image archive in the ecological monitoring and management of a production mangrove forest in Malaysia. *Wetlands Ecology and Management*, *23*, 1049–1066. https://doi.org/10.1007/s11273-015-9443-1

Bosire, J. O., Dahdouh-Guebas, F., Walton, M., Crona, B. I., Lewis, R. R., III, Field, C., … Koedam, N. (2008). Functionality of restored mangroves: A review. *Aquatic Botany*, *89*, 251–259. https://doi.org/10.1016/j.aquabot.2008.03.010

Bunting, P., Clewley, D., Lucas, R. M., & Gillingham, S. (2013). The remote sensing and GIS software library (RSGISLib). *Computers and Geosciences*, *62*, 216–226. https://doi.org/10.1016/j.cageo.2013.08.007

Bunting, P., Rosenqvist, A., Lucas, R. M., Rebelo, L., Hillardes, L., Thomas, N., … Finlayson, C. M. (2018). The global mangrove watch—A new 2010 global baseline of mangrove extent. *Remote Sensing*, *10*, 1669. https://doi.org/10.3390/rs10101669

Chong, V. C. (2006). Sustainable utilization and management of mangrove ecosystems of Malaysia. *Aquatic Ecosystem Health and Management*, *9*(2), 249–260. https://doi.org/10.1080/14634980600717084

Clewley, D., Bunting, B., Shepherd, J., Gillingham, S., Flood, N., Dymond, J., … Moghaddam, M. (2014). A PYTHON-based open source system

for geographic object-based image analysis (GEOBIA) utilising raster attribute tables. *Remote Sensing*, *6*(7), 6111–6135. https://doi.org/10.3390/rs6076111

Costanza, R., d'Arge, R., de Groot, R., Farber, S., Grasso, M., Hannon, B., … van den Belt, M. (1997). The value of the world's ecosystem services and natural capital. *Nature*, *387*(6630), 253–260. https://doi.org/10.1038/387253a0

Dahdouh-Guebas, F., Hettiarachchi, S., Sooriyarachchi, S., Lo Seen, D., Batelaan, O., Jayatissa, L. P., & Koedam, N. (2005). Transitions in ancient inland freshwater resource management in Sri Lanka affect biota and human populations in and around coastal lagoons. *Current Biology*, *15*(6), 579–586. https://doi.org/10.1016/j.cub.2005.01.053

Di Gregorio, A. (2016). Land Cover Classification System. Software version 3. Food and Agriculture Organization of the United Nations. Retrieved from http://www.fao.org/3/a-i5232e.pdf

Di Gregorio, A., & Jansen, L.J.M. (2000). Land Cover Classification System (LCCS): Classification Concepts and User Manual. Environment and Natural Resources Service, GCP/RAF/287/ITA Africover - East Africa Project and Soil Resources, Management and Conservation Service. 179 pages, 28 figures, 3 tables and including CD-ROM. FAO, Rome. 2000.

Di Nitto, D., Neukermans, G., Koedam, N., Defever, H., Pattyn, F., Kairo, J. G., & Dahdouh-Guebas, F. (2014). Mangroves facing climate change: Landward migration potential in response to projected scenarios of sea level rise. *Biogeosciences*, *10*, 857–871. https://doi.org/10.5194/bg-11-857-2014

Duke, N. C., Kovacs, J., Griffiths, A., Preece, L., Hill, J. E., Van Oosterzee, P., … Burrows, D. (2017). Large-scale dieback of mangroves in Australia's Gulf of Carpentaria: A severe ecosystem response, coincidental with an unusually extreme weather event. *Marine and Freshwater Research*, *68*(10), 1816–1829. https://doi.org/10.1071/MF16322

Ellison, A. (2000). Mangrove restoration: Do we know enough? *Restoration Ecology*, *8*, 219–229. https://doi.org/10.1046/j.1526-100x.2000.80033.x

Fatoyinbo, T., Feliciano, E., Lagomasino, D., Lee, S., & Trettin, C. (2017). Estimating mangrove aboveground biomass from airborne LiDAR data: A case study from the Zambezi River delta. *Environmental Research Letters*, *13*, 025012. https://doi.org/10.1088/1748-9326/aa9f03

Fatoyinbo, T. E., & Simard, M. (2013). Height and biomass of mangroves in Africa from ICESat/ GLAS and SRTM. *International Journal of Remote Sensing*, *34*(2), 668–681. https://doi.org/10.1080/01431161.2012.712224

Fatoyinbo, T. E., Simard, M., Washington-Allen, R. A., & Shugart, H. H. (2008). Landscape-scale extent, height, biomass and carbon estimation of Mozambique's mangrove forests with Landsat ETM+ and shuttle radar topography Mission elevation data. *Journal of Geophysical Research*, *113*, G02S06. https://doi.org/10.1029/2007JG000551

Gillingham, S., & Bunting, P. (2014). RFC40: Improving performance of Raster Attribute Table implementation for large tables. Retrieved from http://trac.osgeo.org/gdal/wiki/rfc40_enhanced_rat_support

Goessens, A., Satyanarayana, B., Van der Stocken, T., Zuniga, M. Q., Mohd-Lokmabn, H., Sulong, I., & Dahdouh-Guebas, F. (2014). Is Matang mangrove Forest in Malaysia sustainably rejuvenating after more than a century of conservation and harvesting management. *PLoS One*, *9*(8), e105069. https://doi.org/10.1371/journal.pone.0105069

Hamdan, O., Aziz, H. K., & Hasmadi, I. M. (2014). L-band ALOS PALSAR for biomass estimation of Matang mangroves, Malaysia. *Remote Sensing of Environment*, *155*, 69–78. https://doi.org/10.1016/j.rse.2014.04.029

Hirschmugl, M., Steinegger, M., Gallaun, H., & Schardt, M. (2014). Mapping forest degradation due to selective logging by means of time series analysis: Case studies in Central Africa. *Remote Sensing*, *6*(1), 756–775. https://doi.org/10.3390/rs6010756

Huge, J., Vande Velde, K., Benitez-Capistros, F., Japay, J. H., Satyanarayana, B., Nazrin Ishak, M., … Dahdouh-Guebas, F. (2016). Mapping discourses using Q methodology in Matang Mangrove Forest, Malaysia. *Journal of Environmental Management*, *183*, 988–997. https://doi.org/10.1016/j.jenvman.2016.09.046

Ilman, M., Dargusch, P., Dart, P., & Onrizal. (2016). A historical analysis of the drivers of loss and degradation of Indonesia's mangroves. *Land Use Policy*, *54*, 448–459. https://doi.org/10.1016/j.landusepol.2016.03.010

Kairo, J. G., Dahdouh-Guebas, F., Bosire, J., & Koedam, N. (2001). Restoration and management of mangrove ecosystems—A lesson for and from the east African region. *South African Journal of Botany*, *67*, 383–389. https://doi.org/10.1016/s0254-6299(15)31153-4

Koedam, N., & Dahdouh-Guebas, F. (2008). Ecological quality changes precede changes in quantity in mangrove forests. Science (E-Letter: 02/10/2008). Retrieved from https://www2.ulb.ac.be/sciences/biocomplexity/pub/Koedam&Dahdouh-Guebas_2008_Science.pdf

Komiyama, A., Ong, J. E., & Poungparn, S. (2008). Allometry, biomass, and productivity of mangrove forests: A review. *Aquatic Botany*, *89*, 128–137. https://doi.org/10.1016/j.aquabot.2007.12.006

Lee, S. Y., Primavera, J. H., Dahdouh-Guebas, F., McKee, K., Bosire, J. O., Cannicci, S., … Record, S. (2014). Ecological role and services of tropical mangrove ecosystems: A reassessment. *Global Ecology and Biogeography*, *23*, 726–743. https://doi.org/10.1111/geb.12155

López-Portillo, J., Lewis, R. R., III, Saenger, P., Rovai, A., Koedam, N., Dahdouh-Guebas, F., … Rivera-Monroy, V. H. (2017). Mangrove forest restoration and rehabilitation. In V. Rivera-Monroy S. Lee E. Kristensen & R. Twilley (Eds.), *Mangrove ecosystems: A global biogeographic perspective* (p. 399). Cham, Switzerland: Springer. https://doi.org/10.1007/978-3-319-62206-4_10

Lucas, R. M., Clewley, D., Accad, A., Butler, D., Armston, J., Bowen, M., … Eyre, T. (2014). Mapping forest growth and degradation stage in the Brigalow Belt bioregion of Australia through integration of ALOS PALSAR and LANDSAT-derived foliage projective cover data. *Remote Sensing of Environment*, *155*, 42–57. https://doi.org/10.1016/j.rse.2013.11.025

Lucas, R. M., & Mitchell, A. L. (2017). Integrated land cover and change classifications. In R. Díaz-Delgado, R. Lucas, & C. Hurford (Eds.), *The roles of remote sensing in nature conservation* (Vol. 11, pp. 295–308). Cham, Switzerland: Springer International Publishing.

Lucas, R. M., Mueller, N., Siggins, A., Owers, C., Clewley, D., Bunting, P., … Metternicht, G. (2019). Land cover mapping using digital earth Australia. *Data*, *4*(4), 143. https://doi.org/10.3390/data4040143

Lucas, R. M., Van De Kerchove, R., Otero, V., Lagomasino, D., Fatoyinbo, L., Satyanarayana, B., & Dahdouh-Guebas, F. (2020). Structural characterisation of mangrove forests achieved through combining multiple sources of remote sensing data. *Remote Sensing of Environment*, *237*, 111543. https://doi.org/10.1016/j.rse.2019.111543

Luckman, A., Baker, J., Honzak, M., & Lucas, R. M. (1998). Tropical forest biomass density estimation using JERS-1 SAR: Seasonal variation, confidence limits, and application to image mosaics. *Remote Sensing of Environment*, *63*(2), 126–139. https://doi.org/10.1016/s0034-4257(97)00133-8

Murray, N. J., Phinn, S., DeWitte, M., Ferrari, R., Johnston, R., Lyons, M. B., … Fuller, R. A. (2019). The global distribution and trajectory of tidal flats. *Nature*, *565*, 222–225. https://doi.org/10.1038/s41586-018-0805-8

Otero, V., Lucas, R., Van De Kerchove, R., Satyanarayana, B., Mohd-Lokman, M., & Dahdouh-Guebas, F. (2020). Spatial analysis of early mangrove regeneration in the Matang Mangrove Forest Reserve, peninsular Malaysia, using geomatics. *Forest Ecology and Management* (In press).

Otero, V., Van De Kerchove, R., Satyanarayana, B., Martínez-Espinosa, C., Bin Fisol, M. A., Bin Ibrahim, M. R., … Dahdouh-Guebas, F. (2018). Managing mangrove forests from the sky: Forest inventory using field data and unmanned aerial vehicle (UAV) imagery in the Matang Mangrove Forest Reserve, Peninsular Malaysia. *Forest Ecology and Management*, *411*, 35–45. https://doi.org/10.1016/j.foreco.2017.12.049

Otero, V., Van De Kerchove, R., Satyanarayana, B., Mohd-Lokman, M., Lucas, R., & Dahdouh-Guebas, F. (2019). An analysis of the early regeneration of mangrove forests using Landsat time series in the Matang Mangrove Forest Reserve, Peninsular Malaysia. *Remote Sensing*, *11*(7), 774. https://doi.org/10.3390/rs11070774

Pastor-Guzman, J., Dash, J., & Atkinson, P. (2018). Remote sensing of mangrove forest phenology and its environmental drivers. *Remote Sensing of Environment*, *205*, 71–84. https://doi.org/10.1016/j.rse.2017.11.009

Proisy, C., Viennois, G., Sidik, F., Andayani, A., Enright, J. A., Guitet, S., … Suhardjono . (2018). Monitoring mangrove forests after aquaculture abandonment using time series of very high spatial resolution satellite images: A case study from the Perancak Estuary, Bali, Indonesia. *Marine Pollution Bulletin*, *131*, 61–71. https://doi.org/10.1016/j.marpolbul.2017.05.056

Richards, D. R., & Friess, D. A. (2016). Rates and drivers of mangrove deforestation in Southeast Asia, 2000–2012. *Proceedings of the National Academy of Sciences*, *113*(2), 344–349. https://doi.org/10.1073/pnas.1510272113

Rönnbäck, P., Crona, I., & Ingwall, L. (2007). The return of ecosystem goods and services in replanted mangrove forests: Perspectives from local communities. *Environmental Conservation*, *34*, 313–324. https://doi.org/10.1017/s0376892907004225

Satyanarayana, B., Bhanderi, P., Debry, M., Maniatis, D., Foré, F., Badgie, D., … Dahdouh-Guebas, F. (2012). A socio-ecological assessment aiming at improved forest resource management and sustainable ecotourism development in the mangroves of Tanbi wetland National Park, The Gambia, West Africa. *Ambio*, *41*, 513–526. https://doi.org/10.1007/s13280-012-0248-7

Satyanarayana, B., Van der Stocken, T., Rans, G., Kodikara, K. A. S., Ronsmans, G., Jayatissa, L. P., … Dahdouh-Guebas, F. (2017). Island-wide coastal vulnerability assessment of Sri Lanka reveals that sand dunes, planted trees and natural vegetation may play a role as potential barriers against ocean surges. *Global Ecology and Conservation*, *12*, 144–157. https://doi.org/10.1016/j.gecco.2017.10.001

Shimada, M., Isoguchi, O., Tadono, T., & Isono, K. (2009). PLASAR radiometric calibration and geometric calibration. *IEEE Transaction on Geosciences and Remote Sensing*, *3*, 765–768. https://doi.org/10.1109/TGRS.2009.2023909

Sillanpaa, M., Vantellingen, J., & Friess, D. A. (2017). Vegetation regeneration in a sustainably harvested mangrove forest in West Papua, Indonesia. *Forest Ecology and Management*, *390*, 137–146. https://doi.org/10.1016/j.foreco.2017.01.022

Simard, M., Fatoyinbo, L., Smetanka, C., Rivera-Monroy, V. H., Castañeda-Moya, E., Thomas, N., & Van de Stocken, T. (2018). Mangrove canopy height globally related to precipitation, temperature and cyclone frequency. *Nature Geoscience*, *12*, 40–45. https://doi.org/10.1038/s41561-018-0279-1

Simard, M., Fatoyinbo, L., Smetanka, C., Rivera-Monroy, V. H., Castañeda-Moya, E., Thomas, N., & Van der Stocken, T. (2019). Mangrove canopy height globally related to precipitation, temperature and cyclone frequency. *Nature Geoscience*, *12*, 40–45. https://doi.org/10.1038/s41561-018-0279-1

Spalding, M., Kainuma, M., & Collins, L. (2010). *Word atlas of mangroves* (Vol. 319). London, England: Earthscan.

Tarantino, C., Adamo, M., Lucas, R. M., & Blonda, P. (2016). Detection of changes in semi-natural grasslands by cross correlation analysis with Worldview-2 images and new Landsat-8 data. *Remote Sensing of Environment*, *175*, 65–72. https://doi.org/10.1016/j.rse.2015.12.031

Thomas, N., Lucas, R., Bunting, P., Hardy, A., Rosenqvist, A., & Simard, M. (2017). Distribution and drivers of global mangrove forest change, 1996–2010. *PLoS One*, *12*(6), e0179302. https://doi.org/10.1371/journal.pone.0179302

Verbesselt, J., Hyndman, R., Newnham, G., & Culvenor, D. (2010). Detecting trend and seasonal changes in satellite image time series. *Remote Sensing of Environment*, *114*, 106–115. https://doi.org/10.1016/j.rse.2009.08.014

Walters, B. B., Rönnbäck, P., Kovacs, J. M., Crona, B., Hussain, S. A., Badola, R., … Dahdouh-Guebas, F. (2008). Ethnobiology, socio-economics and management of mangrove forest: A review. *Aquatic Botany*, *89*, 220–236. https://doi.org/10.1016/j.aquabot.2008.02.009

Walton, M. E. M., Samonte-Tan, G. P. B., Primavera, J. H., Edwards-Jones, G., & Le Vay, L. (2006). Are mangroves worth replanting? The direct economic benefits of a community-based reforestation project. *Environmental Conservation*, *33*(4), 335–343. https://doi.org/10.1017/S0376892906003341

Weidmann, N. B., Kuse, D., & Gleditsch, K. S. (2010). The geography of the international system: The CShapes dataset. *International Interactions*, *36*(1), 86–106. https://doi.org/10.1080/03050620903554614

Wessel, B. (2016). TanDEM-X ground segment – DEM products specification document, EOC, DLR, Oberpfaffenhofen, Germany, public document TD-GS-PS-0021, issue 3.2, 2018. Available from https://tandemx-science.dlr.de/.

Worthington, T., & Spalding, M. (2018). Mangrove restoration Potential: A global map highlighting a critical opportunity. https://doi.org/10.17863/CAM.39153

How to cite this article: Lucas R, Otero V, Van De Kerchove R, et al. Monitoring Matang's Mangroves in Peninsular Malaysia through Earth observations: A globally relevant approach. *Land Degrad Dev*. 2020;1–20. https://doi.org/10.1002/ldr.3652